1961-05-01

Investigation of dry friction phenomena in rotary sliding vane machinery

Masalin, Charles Ero; Taylor, James M.

Massachusetts Institute of Technology

http://hdl.handle.net/10945/12411

INVESTIGATION OF DRY FRICTION PHENOMENA IN ROTARY SLIDING VANE MACHINERY

CHARLES ERO MASALIN
and
EDWARD G. OGDEN

INVESTIGATION OF DRY FRICTION PHENOMENA IN ROTARY SLIDING VANE MACHINERY

by

CHARLES ERO MASALIN, LIEUTENANT, U.S. NAVY
B.S., U.S. Naval Academy
(1955)

and

EDWARD G. OGDEN, LIEUTENANT, U.S. NAVY
B.S., U.S. Naval Academy
(1955)

SUBMITTED IN PARTIAL FULFILLMENT OF THE REQUIREMENTS
FOR THE MASTER OF SCIENCE DEGREE IN NAVAL ARCHITECTURE
AND MARINE ENGINEERING AND THE
PROFESSIONAL DEGREE, NAVAL ENGINEER
at the
MASSACHUSETTS INSTITUTE OF TECHNOLOGY
May, 1961

Signature of Authors: ____________________________________

____
Department of Naval Architecture and
Marine Engineering, 20 May 1961

Certified by: ____________________________________
Thesis Supervisor

Accepted by: ____________________________________
Chairman, Departmental Committee
on Graduate Students

INVESTIGATION OF DRY FRICTION PHENOMENA IN ROTARY SLIDING VANE MACHINERY

by

Lt. Charles Ero Masalin, U.S.N. and Lt. Edward G. Ogden, U.S.N.

Submitted to the Department of Naval Architecture and Marine Engineering on 20 May 1961 in partial fulfillment of the requirements for the Master of Science Degree in Naval Architecture and Marine Engineering and the Professional Degree of Naval Engineer.

ABSTRACT

The purpose of this report is to isolate the various modes of friction in a "dry" rotary sliding vane machine and to determine the influence of pressure, temperature, and speed on these modes of friction.

A pressure transducer was mounted in a rotary sliding vane pump rotor and a thermocouple in a vane to note effects of pressure and temperature, respectively. The rotor end plates were machined to permit mounting the rotor eccentric and concentric to determine the effects of vane movement within the rotor and to determine coefficients of sliding friction. Holes were also machined in the end plates to eliminate pressure effects.

Results show that vane movement against the casing and within the rotor represents a significant amount of the total power input, their sum being greater than 50 percent at higher speeds. Theoretical formulations coupled with experimental results show that temperature and normal forces on the vanes had a negligible effect on the coefficients of friction. Because friction increases exponentially with speed, a "dry" rotary sliding vane pump is limited to a relatively low speed range.

Calculations based on theoretical formulations as derived in this paper used in conjunction with experimental data of this paper show a reduction in friction power of a proposed design when low friction vane materials are used and when the vanes are located radially within the rotor. Hence, these calculations show trends in improving machine efficiency.

Thesis Supervisor: Brandon G. Rightmire
Title: Professor of Mechanical Engineering

ACKNOWLEDGEMENTS

The authors wish to express their appreciation to Professor B. G. Rightmire for his extensive advice and time. The authors wish also to express an indebtedness to Messrs. E. M. Herrmann and R. C. Bartlett at the Naval Engineering Experiment Station, Annapolis, Maryland for their aid in procurement of essential instrumentation and to Mr. Davis Spencer of M-D Blowers, Inc. for supplying the experimental pump.

TABLE OF CONTENTS

LIST OF FIGURES

LIST OF FIGURES (cont'd.)

LIST OF TABLES

Number Page

TABLE OF SYMBOLS

A	Used in referring to exposed vane area (sq.inches)
D_c	Cylinder bore diameter (inches)
D_r	Rotor diameter (inches)
e	Rotor eccentricity (inches)
F_a	Component for one vane of the force due to total acceleration acting along the vane with the rotor eccentric (pounds)
F_c	Force for one vane due to total acceleration acting along R_g with rotor eccentric (pounds)
F_r	Resultant force for one vane with rotor eccentric and a pressure difference across the vane acting at the point of contact of the vane end and cylinder bore and directed along R_v (pounds)
F_{rd}	Resultant force for one vane with no pressure influence and rotor eccentric acting at point of contact between vane and cylinder bore along R_v (pounds)
f_{rf}	Coefficient of friction for the reciprocating vane motion within the rotor slot
f_{sf}	Coefficient of friction for the vane sliding against the casing
G_c	Component for one vane of the centrifugal force acting along vane with rotor concentric (pounds)
h	Average vane extension out of rotor with rotor eccentric (inches)
h_c	Vane extension out of rotor with rotor concentric (inches)
H_c	Component of force for one vane, due to total acceleration when the rotor is eccentric, acting normal to the vane at the vane center of gravity (pounds)
H_p	Pressure force acting normal to one vane with rotor eccentric (pounds)
H_{rd}	Resultant force for one vane normal to the vane and acting at the vane end in contact with the cylinder bore with no pressure influence and rotor eccentric (pounds)

I_{cd}	Resultant force acting at point of contact of vane and cylinder bore along R_{vc}, for one vane with rotor concentric (pounds)
l	Vane length (inches)
l_c	Cylinder bore length (inches)
N	Pump speed with rotor eccentric (revolutions per minute)
N_c	Pump speed with rotor concentric corresponding to N such that $V_c = V$ (revolutions per minute)
$(P_i)_n$	Power measured at pump speed N as measured in Experiments 1, 3, and 4 $(i = 1, 3, \text{ or } 4)$ (horsepower)
$(P_j)_{nc}$	Power measured at pump speed N_c as measured in Experiments 2 and 5 $(j = 2 \text{ or } 5)$ (horsepower)
$(P_{sf})_n$	Power dissipated in overcoming sliding friction of vanes against casing with rotor eccentric and a pressure difference across the vanes at pump speed N (horsepower)
$(P_{sfd})_n$	Power dissipated in overcoming sliding friction with no pressure influence and rotor eccentric at pump speed N (horsepower)
$(P_{sfd})_{nc}$	Power dissipated in overcoming sliding friction with no pressure influence and rotor concentric at pump speed N_c (horsepower)
$(P_{rf})_n$	Power dissipated in overcoming reciprocating friction with rotor eccentric and a pressure difference across the vanes at pump speed N (horsepower)
$(P_{rfd})_n$	Power dissipated in overcoming reciprocating friction with no pressure influence and rotor eccentric at pump speed N (horsepower)
R_1	Reaction force, for one vane with rotor eccentric, acting normal to a vane at the vane end in the slot when there is no pressure difference across the extended portion of the vane (pounds)
R_2	Reaction force, for one vane with rotor eccentric, acting normal to a vane at the rotor radius when there is no pressure difference across the extended portion of the vane (pounds)
R_3	Reaction force for one vane with rotor eccentric and a pressure difference across the vane acting normal to the vane at the vane end in the slot (pounds)

R_4	Reaction force for one vane with rotor eccentric and a pressure difference across the vane acting normal to the vane at the rotor radius (pounds)
R_g	Average radius to vane center of gravity with rotor eccentric (inches)
R_{gc}	Radius to vane center of gravity with rotor concentric (inches)
R_v	Average radius to vane end with rotor eccentric (inches)
R_{vc}	Radius to vane end with rotor concentric (inches)
t	Vane thickness (inches)
V	Average vane end velocity with rotor eccentric (feet per second)
V_c	Vane end velocity with rotor concentric (feet per second)
V_r	Average vane reciprocating velocity with rotor eccentric (feet per second)
w	Weight of one vane (pounds)
z	Vane width (inches)
α	Angle between rotor radius and the vane slots (degrees)
β	Angle between R_g and the vane slots (degrees)
β_c	Angle between R_{gc} and the vane slots (degrees)
λ	Angle between R_v and vane (degrees)
λ_c	Angle between R_{vc} and the vane (degrees)
Δp	Used in referring to pressure differential across vanes (pounds per sq. inch)

I. INTRODUCTION

Basic Concept

A dry rotary sliding vane machine is basically a positive displacement device consisting of a rotor mounted eccentric in a cylinder. Vanes are mounted in the rotor and are held against the cylinder bore by centrifugal force. Sometimes the vanes are spring loaded to ensure their contact with the cylinder bore at slower speeds. Expansion and compression of the gaseous working fluid is realized by the rotor being mounted eccentric within the cylinder. Inlet and exhaust ports are located most often in the casing end plates to permit the working fluid to enter into and exhaust from the volume bounded by the rotor, casing, and vanes--the inlet port being exposed to the low pressure region of the cycle. The degree of eccentricity will ideally determine the pressure ratio for a given size device. The vanes sweeping past the inlet and exhaust ports provide a simple valving configuration. However, a cyclic analysis is complicated by this arrangement when portions of the working fluid are exposed simultaneously to conditions at inlet and exhaust. This, of course, depends upon port location and the number of vanes mounted in the rotor. Eccentricity also determines the rotary sliding vane machine's capacity. In the absence of shaft seals, the capacity is limited by the allowed leakage through the shaft and rotor end clearances. Eccentricity and port location further determine the amount of working fluid carried over to the succeeding cycle.

The basic machine has very few moving parts--the vanes

sliding within the rotor, the rotor rotating within the casing. Because the machine is so very simple, it occupies minimum space and weighs little when compared with other types of pumps of equal capacity and pressure ratio.

Types

Rotary sliding vane machinery has applications as either a pump or a motor. For pumping applications it is used as a vacuum priming pump, a low-capacity refrigeration compressor, and in several industrial applications requiring low-capacity, low-pressure air or other gases. The most recent application of the rotary vane machine as a motor is the Wankel engine.[6] However, applications using the rotary sliding vane machine as a pump rather than a motor predominate. Careful note should be made that this study deals with "dry" rotary sliding vane machinery in contrast to the "wet" type. The "dry" machine is unique in that it requires no fluid (oil, water, etc.) to seal the contact area between the vanes and cylinder bore when the working fluid is gaseous. The sealing fluid also serves to reduce the sliding friction. The"wet" pump utilizing the sealing fluid is by necessity larger and more complex since it requires a means of fluid supply as well as a fluid reservoir.

Frictional Considerations

Intuitively, if by no other consideration, one may feel that the dry friction of the sliding vanes against the rotor and the cylinder bore would certainly hinder the rotary sliding vane machine in any economical pumping consideration. Unfortunately, the literature holds no detailed friction

analysis of this type of machine. Consequently, no one can say just what the optimum design considerations relating to the friction characteristics might be. Some study has been devoted to other component considerations of the rotary sliding vane machine[4] such as the effects of overcompression caused by varying the inlet and exhaust port location and the ideal relationships between volumetric efficiency, compression ratio, and rotational speed.

It will be the purpose of this report to conduct a friction analysis of a rotary sliding vane machine in order that a better over-all design may be realized. Theoretical formulations will be developed where deemed appropriate. Of necessity, however, an experimental technique will be developed to show the applicability of the theoretical formulations and, in the end, to show what the actual frictional characteristics are for the machine investigated.

Experimental Equipment

For experimental work, a rotary sliding vane machine manufactured by M-D Blowers, Inc. of Racine, Wisconsin and intended primarily for use as a vacuum priming pump was selected since it represents a typical design. The pump consists of a gray cast-iron cylindrical casing within which is mounted at an eccentricity of 0.3715 inches a gray cast-iron rotor. The rotor is cast onto a steel shaft. The base of the pump is an integral part of the cylinder casing. The cylindrical casing is tapped on both sides at the middle of the transverse section for inlet and exhaust connections. The end plates are of gray cast-iron and are secured to the

casing by eight machine screws. Inlet and exhaust ports are contained within these end plates as well as the housings for the two rotor shaft bearings. The bearings are mounted in a counterbore and are positioned by a screw-fastened closure washer and a shoulder on the shaft. The rotor is machined to hold four carbon graphite vanes in slots that are cut at an angle of 38 degrees from the radial position. Felt shaft seals are mounted in the end plates next to the rotor and thereby keep the end leakage flow to a minimum. Clearance between the rotor and the end plates is approximately 0.002 inches. Clearance between the rotor and the cylinder bore at top dead center is approximately 0.005 inches. External to the pump are located pressed steel fans mounted on the shaft which direct cooling air on the two end plates to cool the bearings. In the suction line is located a sponge-type filter mounted in a steel case to exclude foreign matter from the pump to preclude vane failures. Figures I, II, and III show detailed pump characteristics. Additional principal dimensions not shown in Figure III include:

Cylinder bore diameter, D_c	4.601 inches
Cylinder length, l_c	6.223 inches
Rotor diameter, D_r	3.855 inches
Rotor and vane length, l	6.219 inches
Vane width, z	1.6875inches
Vane thickness, t	0.180 inches

Figure I

M-D Dri-Air Pump, Model 6

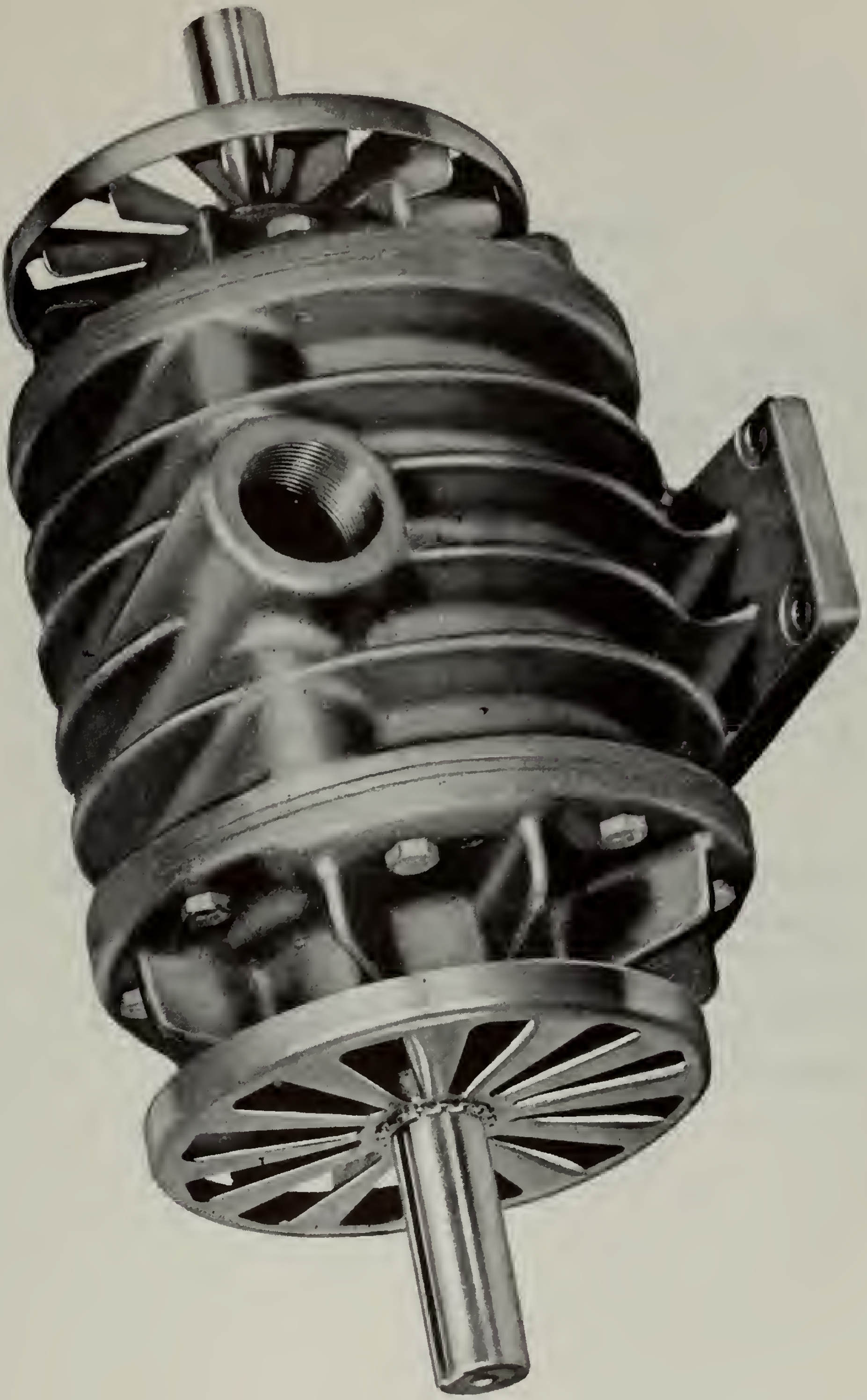

Courtesy of
M-D Blowers, Inc.

Figure II

Pump Components and Characteristics

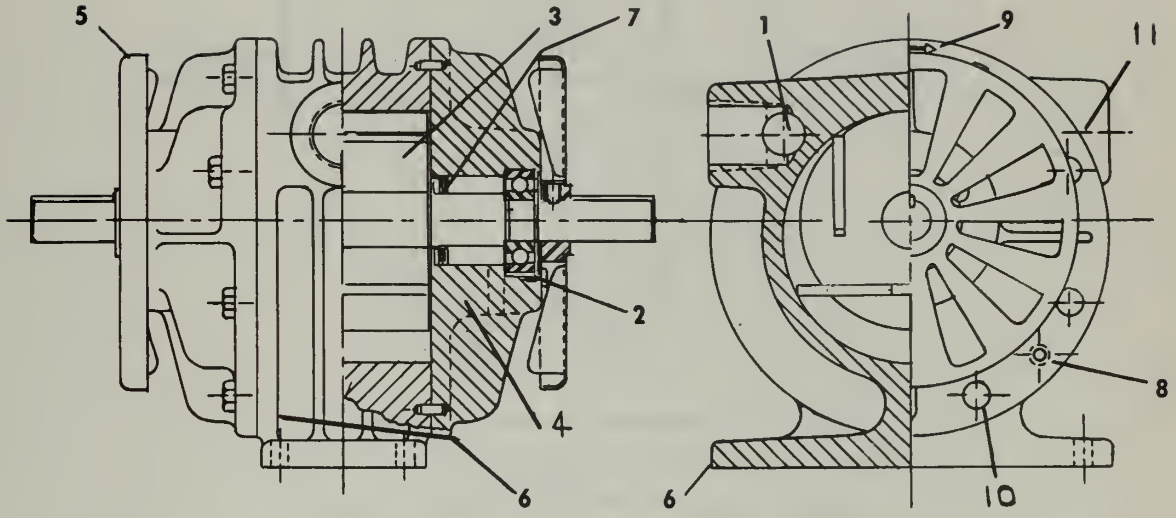

Part Number	Description
1	Exhaust Connection
2	Shaft Bearings
3	Rotor
4	End Plate
5	Cooling Fan
6	Casing and Integral Base

Part Number	Description
7	Shaft Seal
8	Tapped Holes for Disassembly Jack Screws
9	Direction of Rotation
10	Holes for End Plate Mounting
11	Inlet Connection

Figure III

Pump Dimensions

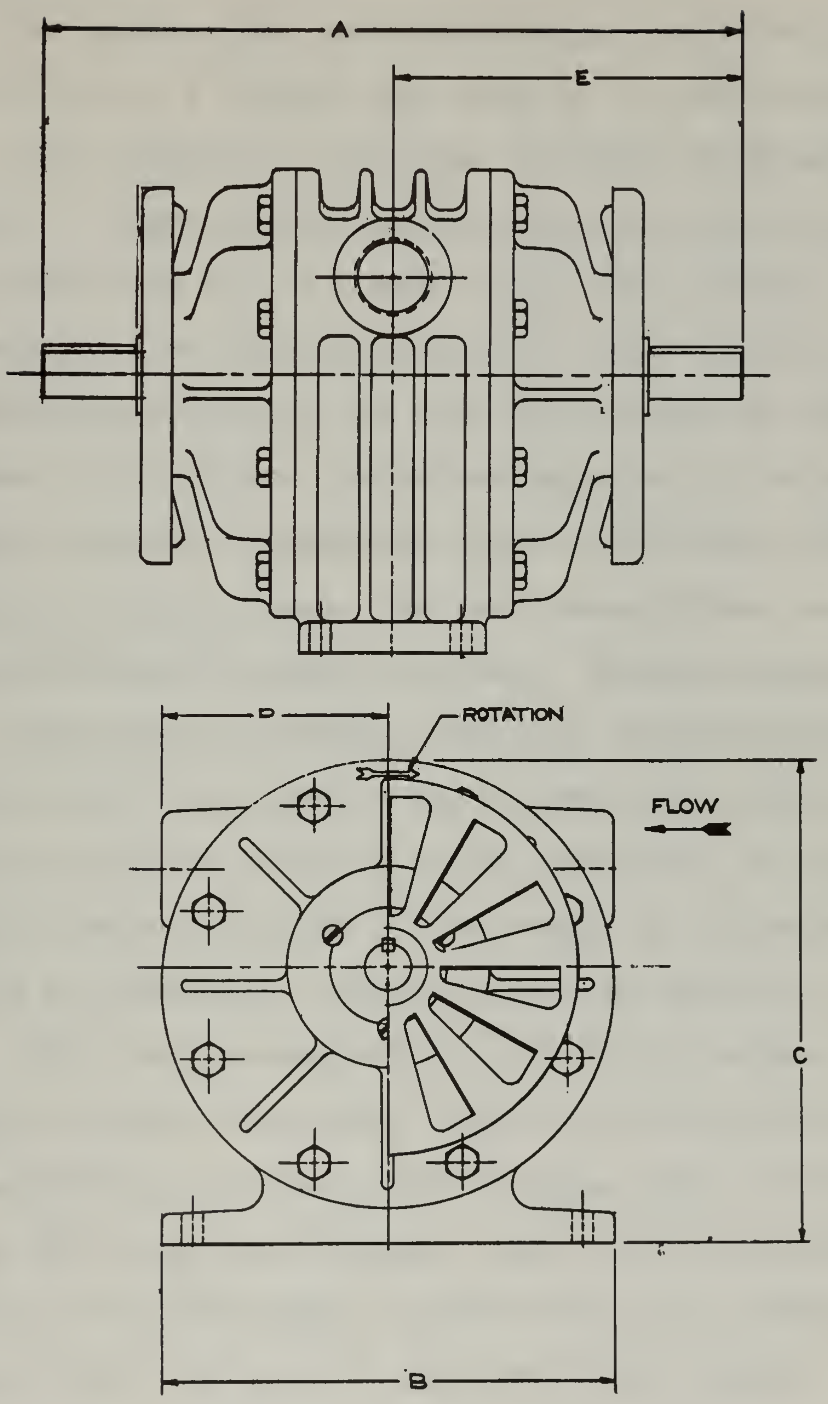

A = 17.25 inches
C = 7.875 inches
B = 7.25 inches
D = 3.625 inches
E = 8.625 inches

[illegible]

[illegible]

[illegible]

[illegible]

II. PROCEDURE

Friction Analysis

From our preliminary investigation of the frictional characteristics of a rotary vane machine, it was determined that the power required to overcome friction is dissipated by two means. There is the sliding friction acting at the vane ends when they are in contact with the cylinder, hereafter referred to as sliding friction. There is also the sliding friction acting on the vane as it moves in and out of the slots in the rotor, hereafter referred to as reciprocating friction. These two modes of friction are affected by the rotor speed, the vane temperature, and the pressure differential across the vane. The most precise method of analyzing the various friction characteristics is by an experimental technique. To determine the effect of each of the variables involved which contribute to the overall friction characteristics of this pump, it is necessary to separate the variables affecting the two modes of sliding friction. This was accomplished by altering the pump configuration so that each effect could be studied separately and its contribution to the total friction power found. In the rotary vane pump investigated, this was accomplished in a series of five experiments in which the rotor position was changed, and also the type of end plate was changed. The pump configuration and effect studied in each experiment are shown in the following table:

Experiment Number	Rotor Position	Type of End Plate	Mode of Friction	Included Effects
1	Concentric	Closed	Bearing and Seal	Speed (vanes removed)
2	Concentric	Closed	Bearing, Seal, and Sliding	Speed and Temperature
3	Eccentric	Closed	Bearing, Seal, Reciprocating, and Sliding	Speed, Pressure, and Temperature
4	Eccentric	Open	Bearing, Seal, Reciprocating, and Sliding	Speed and Temperature
5	Concentric	Open	Bearing, Seal, and Sliding	Speed and Temperature

Measurement Procedure

The pump was mounted so that it was driven by a dynamometer to determine the power required. Power was calculated by measuring the torque exerted by the dynamometer. The dynamometer used had a 0.5-foot radius arm. The force at this radius arm was measured with a spring scale which was calibrated with standard weights. The dynamometer speed was measured with a three-second tachometer. The power was found using the formula

$$P = \text{Force} \times \text{Speed} \times 0.5 \times \frac{2\pi}{60} \times \frac{1}{550} \qquad (1)$$

The dynamometer speed was controlled by a rheostat in series with the shunt field of the direct current dynamometer. The inlet vacuum to the pump was measured by use of a mercury manometer and was controlled by use of an inlet throttle valve. The pressure differential across the vanes was measured by mounting a pressure transducer in the rotor in between two vanes and connecting the transducer output to an

oscilloscope. For analysis purposes pictures of the scope presentations were taken at four speeds for two values of inlet pressure. The scope scale factor and the transducer calibration curve enabled the conversion of the scope deflections to a pressure difference across a vane for any rotor position. The vane temperature was measured by mounting a copper-constantan thermocouple in a vane as near as possible to the sliding surface at the vane end. The thermocouple voltage was led to a Sanborn recorder through copper slip rings mounted on an extension of the pump rotor shaft. The use of slip rings required a compensating network to eliminate the Peltier effect. The network used is due to Z. J. J. Stekly.[14]

The experimental set-up is shown in Figures IV, V, and VI. Speed and power were measured during each experiment. Inlet vacuum was varied for Experiment 3, and the pressure differential across the vanes was measured for this experiment only, since it was negligible or eliminated in the other experiments. Vane temperatures were measured only during Experiment 5 due to the vane strength limitations which resulted in vane failures during other experiments when it was attempted to install a thermocouple in a vane. However, since the vane temperature is dependent to a large degree upon the speed of the rubbing surfaces, the temperature variation measured in Experiment 5 will closely approximate that of the other experiments at corresponding speeds. In those experiments in which pumping effects have been eliminated, there is no temperature rise due to compression; however, with no pumping, there is no cooling fluid passing through the machine

Figure IV

Pressure Transducer and Thermocouple Installation

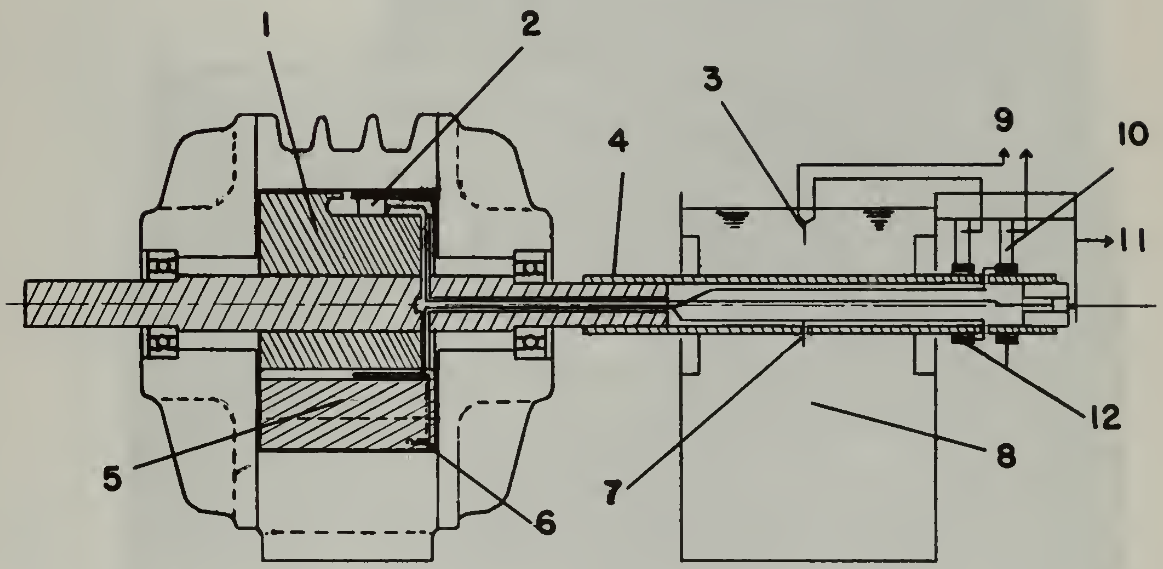

1. Rotor
2. Pressure Transducer
3. Compensating Thermocouple
4. Shaft Extension
5. Vane
6. Thermocouple mounted in Vane
7. Compensating Thermocouple
8. Water Bath
9. Thermocouple Output
10. Copper Brushes
11. Pressure Transducer Output
12. Copper Slip Rings

Figure V

Experimental Set-up

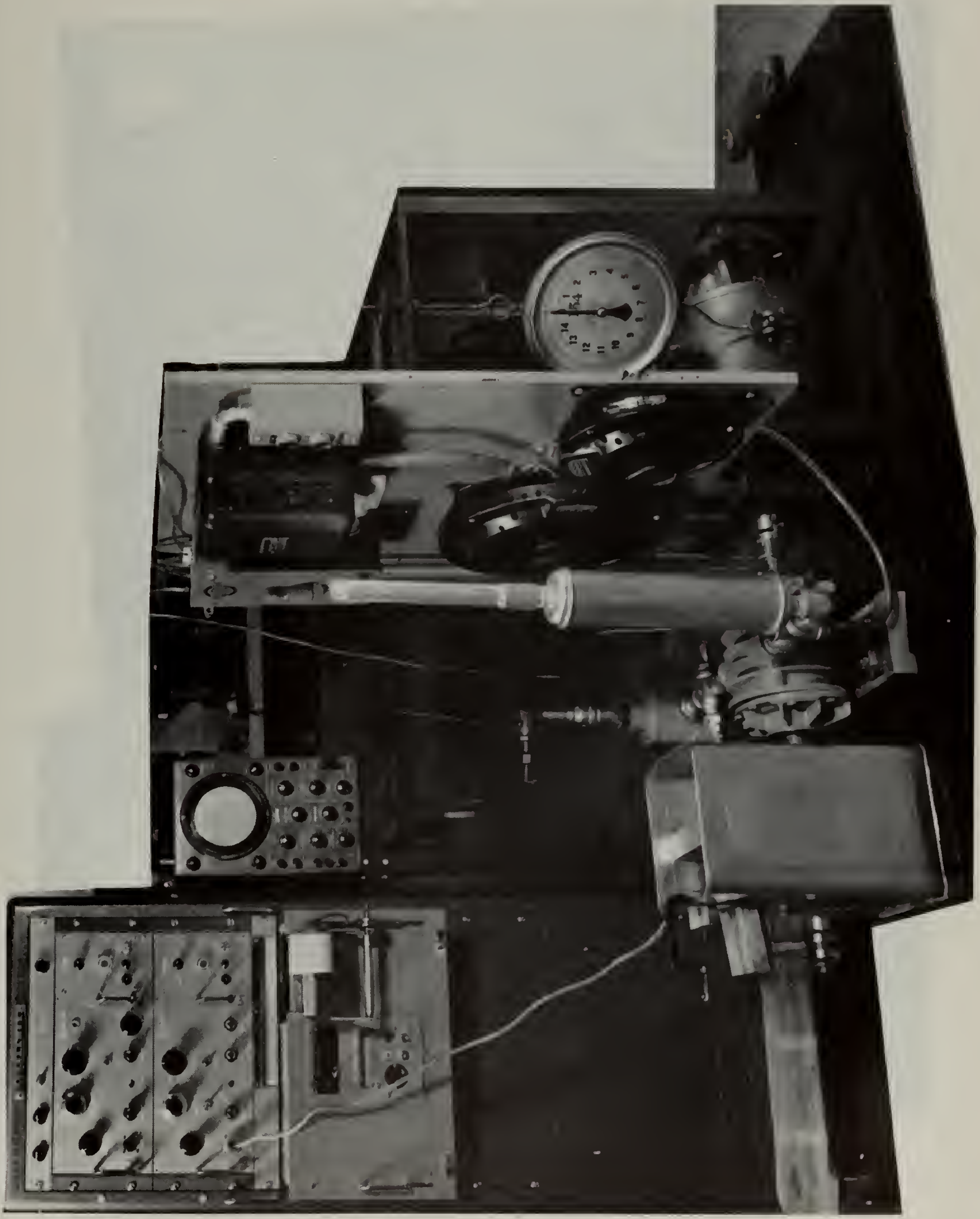

Figure VI

Close view of Experimental Set-up

to cause a cooling effect on the vanes. Hence, the effects of no pumping resulting in no fluid flow tend to counteract each other as far as the vane temperature is concerned and, therefore, the temperature variation found in Experiment 5 is indicative of the trend of the temperature variation in the other experiments. The speed range investigated in these experiments was from 1000 rpm to 1500 rpm, which is the range of normal pump operation. The inlet vacuum was set at 5 or 10 inches of mercury. Higher inlet vacuums were unattainable due to the power limitation of the dynamometer.

Data Analysis

In order to obtain the fraction of power dissipated by the two modes of friction during normal pump operation, it was necessary to correlate the data taken in the concentric configuration to the eccentric configuration to make it applicable to the normal pump operation. The normal pump configuration is that used in Experiment 3. When the pump is operating with the rotor eccentric, the vane end radius, the vane exposure, the radius to the vane center of gravity, the angle between the radius to the vane center of gravity and the vane slots, and the angle between the vane end radius and the vane are all varying quantities dependent upon rotor position. The average value of these quantities for one revolution with the rotor eccentric was used as the basis of correlation with the corresponding values of these quantities when the rotor was placed concentric. The average was used since the measured power represents an average power per revolution. When the rotor is mounted concentric, these

quantities have constant values and are independent of rotor position. From a drawing of the cylinder bore with the rotor eccentric the quantities were measured at fifteen-degree intervals for one revolution, and the average values found are:

R_v = 2.2818 inches
h = 0.4229 inches
R_g = 1.6325 inches
β = 47.5 degrees
λ = 32.0 degrees

These values were obtained by the procedure outlined in Appendix A.1. The values for these quantities with the rotor concentric are:

R_{vc} = 2.3005 inches
h_c = 0.4600 inches
R_{gc} = 1.6450 inches
β_c = 46.0 degrees
λ_c = 31.0 degrees

In order to make $V = V_c$, it is necessary to run the pump at a slower rpm in the concentric configuration than in the eccentric configuration since $R_{vc} > R_v$. For the condition $V = V_c$:

$$N_c = \frac{R_v \text{ x } N}{R_{vc}} = \frac{N}{1.0082} \tag{2}$$

and
$$V_c = \left(\frac{2\pi N_c}{60}\right)\left(\frac{R_{vc}}{12}\right) = V = \left(\frac{2\pi N}{60}\right)\left(\frac{R_v}{12}\right) \tag{3}$$

Since the coefficient of friction is a function of speed and temperature in our experiments, it is necessary to calculate the coefficient of sliding friction, f_{sf}, at the speed N_c from the data of Experiment 2 for use in calculating the power dissipated by sliding friction in Experiments 3 and 4 at the speed N. The change in coefficient of friction might be more properly related to a change at various speeds in the normal force against the vane acting at the point of contact.

However, with changes in normal force, this variation in the coefficient of friction is negligible[1]; hence it is assumed that f_{sf} as calculated for a given velocity from Experiment 2 is the coefficient of friction for carbon graphite on cast iron for that velocity for the eccentric configurations where there are increases of the normal force by a factor of 5 or less. To determine f_{sf} from Experiment 2 it is necessary only to find the normal force acting at the point of contact with the cylinder bore, since the power and velocity are measured quantities. The power required to overcome sliding friction when the rotor is concentric is:

$$(P_{sfd})_{nc} = (P_2)_{nc} - (P_1)_n \qquad (4)$$

$$(P_{sfd})_{nc} = 4\ f_{sf}\ I_{cd}\ V_c/550 \qquad (5)$$

Multiplication by four is necessary since I_{cd} is determined for one vane only. The normal force can be found by summing the forces acting along the vane. (See Figure VII.)

$$G_c + f_{sf}\ I_{cd} \sin \lambda_c = I_{cd} \cos \lambda_c \qquad (6)$$

where G_c is the component of the centrifugal force along the vane.

$$G_c = \frac{W}{g} \times \left(\frac{2\pi N_c}{60}\right)^2 \times \frac{R_{gc}}{12} \cos\beta_c \qquad (7)$$

Rewriting Equation 5,

$$f_{sf}\ I_{cd} = \frac{137.5\ (P_{sfd})_{nc}}{V_c} \qquad (8)$$

hence,

$$I_{cd} = \frac{G_c}{\cos\lambda_c} + \frac{137.5(P_{sfd})_{nc} \tan \lambda_c}{V_c} \qquad (9)$$

All the quantities except I_{cd} in Equation 9 are known so that I_{cd} can be determined. This enables f_{sf} to be computed.

The procedure to calculate the coefficient of reciprocating

[illegible]

$$[illegible]$$

$$[illegible]$$

$$[illegible]$$

[illegible]

$$[illegible]$$

[illegible]

$$[illegible]$$

$$[illegible]$$

[illegible]

Figure VII

Dimensions and Forces with Rotor Concentric

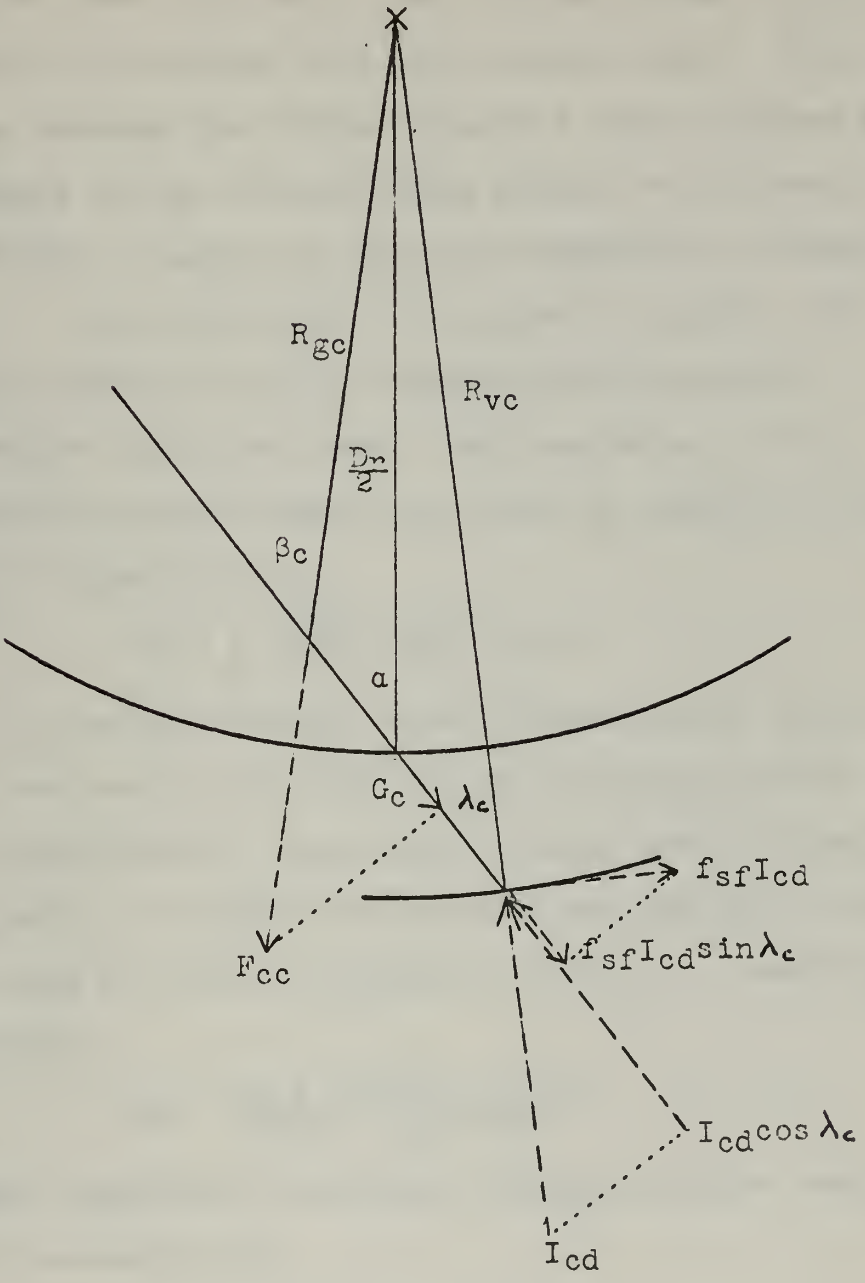

R_{gc} = 1.645 in. α = 38 degrees

R_{vc} = 2.3005 in. β_c = 46 degrees

$D_r/2$ = 1.9275 in. λ_c = 31 degrees

friction is essentially the same but is more involved. When the vane is moving in and out of the vane slots as the rotor is rotating, there are two forces acting normal to the vane within the vane slot and a force acting normal to the vane where it is in contact with the cylinder bore. These can be found by summing the forces along the vane and then summing the moments of the forces acting normal to the vane. (See Figure VIII.) Along the vane the summation of forces is:

$$F_a = F_{rd} (\cos\lambda - f_{sf} \sin\lambda) - f_{rf}(R_1 + R_2) \qquad (10)$$

F_a is the force due to the component of the total acceleration along the vane. The resolution of the accelerations present when the rotor is eccentric is explained in Appendix A.2.

$$F_a = \frac{w}{g} \left(\frac{2\pi N}{60}\right)^2 \left(\frac{R_g}{12}\right) \cos\beta \qquad (11)$$

R_1 and R_2 are the average normal forces acting on the vane at the vane end in the slot and at the outer end of the vane slot, respectively. F_{rd} is the average normal force acting at the point of contact of the vane end and the cylinder casing when the rotor is mounted eccentric. Rewriting Equation 10,

$$F_{rd} = \frac{F_a + f_{rf} (R_1 + R_2)}{\cos\lambda - f_{sf} \sin\lambda} \qquad (12)$$

The power required to overcome sliding friction when the rotor is eccentric is:

$$(P_{sfd})_n = 4 f_{sf} F_{rd} V/550 \qquad (13)$$

$$(P_{sfd})_n \neq (P_{sfd})_{nc} \text{ since } F_{rd} \neq I_{cd}$$

The power required to overcome reciprocating friction is:

$$(P_{rfd})_n = (P_4)_n - (P_1)_n - (P_{sfd})_n \qquad (14)$$

Figure VIII

Dimensions and Forces with Rotor Eccentric

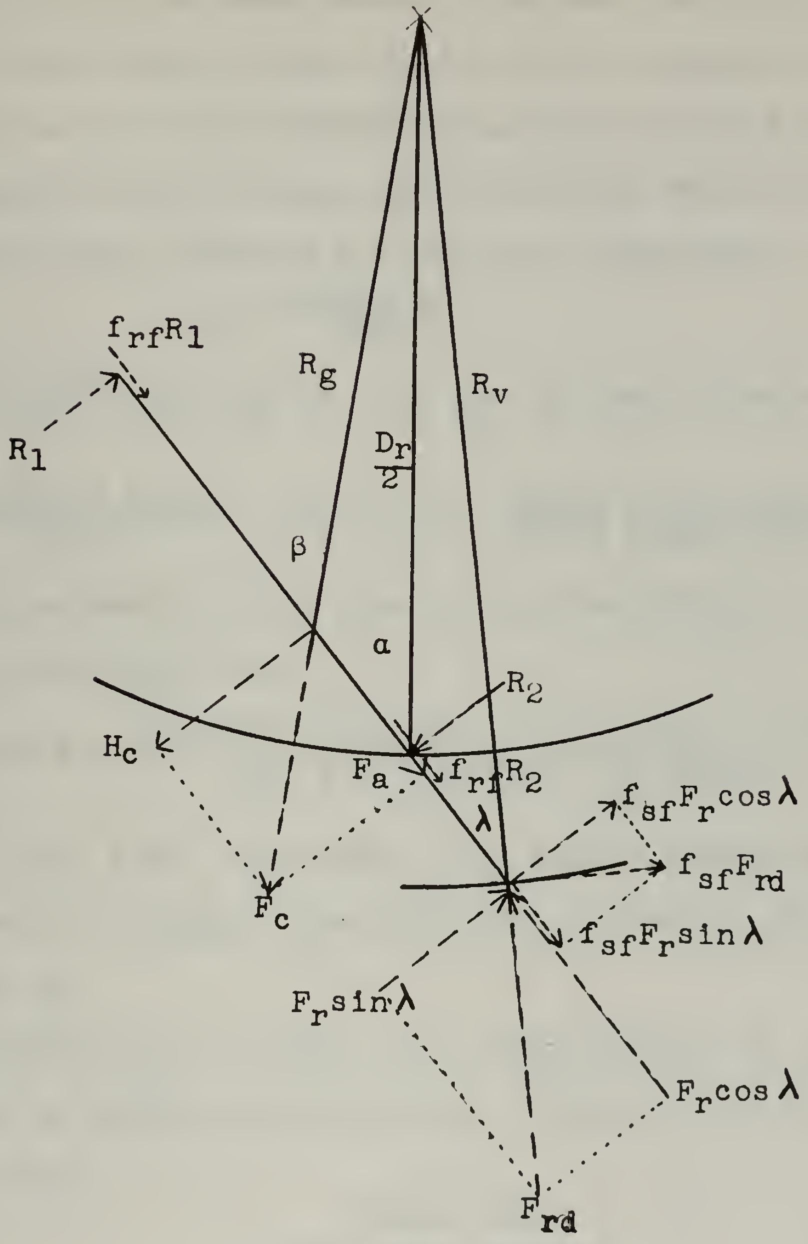

R_g = 1.6325 in.
R_v = 2.2818 in.
$D_r/2$ = 1.9275 in.

α = 38 degrees
β = 47.5 degrees
λ = 31 degrees

and also,

$$(P_{rfd})_n = 4\ f_{rf}\ (R_1 + R_2)\ V_r/550 \qquad (15)$$

V_r is the average velocity of the vane when it is moving into or out of the vane slots. This was found by taking the distance the vane can move from the full extended vane position to the full retracted vane position and dividing by the time for this distance to be traveled which is approximately the time required for one-half revolution.

$$V_r = \frac{N e \sec\ \lambda}{180} \qquad (16)$$

Substituting Equations 12, 13, and 15 into Equation 14, we have

$$\frac{f_{rf}(R_1 + R_2)V_r}{137.5} = (P_4 - P_1)_n - \frac{f_{sf}V}{137.5}\left[\frac{F_a + f_{rf}(R_1 + R_2)}{\cos\lambda - f_{sf}\ \sin\lambda}\right] \qquad (17)$$

The only unknown in this equation is the product $f_{rf}(R_1+R_2)$. Solving for $f_{rf}(R_1 + R_2)$:

$$f_{rf}(R_1+R_2) = \frac{137.5(P_4 - P_1)(\cos\lambda - f_{sf}\ \sin\lambda) - f_{sf}V\ F_a}{f_{sf}\ V + V_r(\cos\lambda - f_{sf}\ \sin\lambda)} \qquad (18)$$

With $f_{rf}\ (R_1 + R_2)$ calculated, F_{rd} can be computed from Equation 12; $(P_{sfd})_n$, from Equation 13; and $(P_{rfd})_n$, from Equation 15.

Now that F_{rd} is known, the normal forces R_1 and R_2 can be found as previously described. Using a free body diagram of the vane,

Figure IX

Free Body Diagram

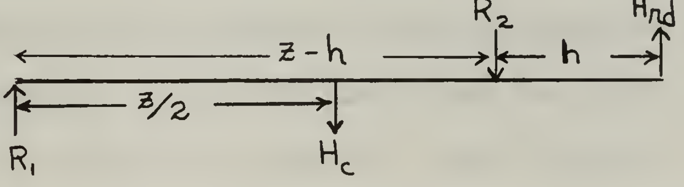

$$R_1 + R_2 = 1.6688\ H_{rd} - 0.3344\ H_c \qquad (19)$$

The derivation of this equation is explained in Appendix A.3. H_{rd} is the total normal force due to F_{rd} and is expressed as

$$H_{rd} = F_{rd} \ (\sin\lambda + f_{sf} \cos\lambda) \tag{20}$$

H_c is the component of the force due to the total acceleration normal to the vane.

$$H_c = \frac{w}{g} \left(\frac{2\pi N}{60}\right)^2 \left(\frac{R_g}{12}\right) \sin \beta \tag{21}$$

Knowing $R_1 + R_2$, f_{rf} can be found by,

$$f_{rf} = \frac{f_{rf} \ (R_1 + R_2)}{(R_1 + R_2)} \tag{22}$$

Now that f_{sf} and f_{rf} can be determined for any desired speed, the power required to overcome sliding friction and reciprocating friction at the same speed when the pump is operating in its normal configuration can be calculated by accounting for the influence of the pressure differential across a vane when the pump is actually pumping. The average pressure difference across a single vane is found by analyzing the scope presentations of the pressure transducer output. The procedure for finding the pressure difference and the force due to the pressure difference is outlined in Appendix A.4.

The influence of the pressure difference across a vane appears as a change in the normal forces acting on the vane in the vane slot and as a change in the normal force at the point of contact of the vane end and the cylinder bore.

Again we use the procedure that was used in determining f_{rf}. The summation of the forces along the vane is

$$F_a = F_r \ (\cos\lambda - f_{rf} \sin\lambda) - f_{rf} \ (R_3 + R_4) \tag{23}$$

where F_r and $R_3 + R_4$ are forces similar to F_{rd} and $R_1 + R_2$.

These new forces are greater due to an additional force, H_p, which is the average effective pressure force acting on each vane during one revolution and acts at the center of the average vane exposure as shown in Figure X.

Since Equation 23 poses two unknown quantities, F_r and $R_3 + R_4$, another relationship of these two unknowns must be used to calculate these forces. By using a free body diagram of the vane and summing the moments of the forces acting, we have

$$R_3 + R_4 = 1.6688(\sin\lambda + f_{sf} \cos\lambda)F_r + 1.3344\, H_p - 0.3344 H_c \quad (24)$$

The derivation of this equation is given in Appendix A.5.

Figure X

Free Body Diagram

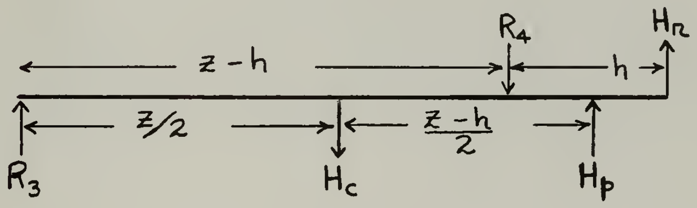

Substituting Equation 24 into Equation 23

$$F_r = \frac{F_a + 1.3344 f_{rf}\, H_p - 0.3344 f_{rf}\, H_c}{(\cos\lambda + f_{sf} \sin\lambda) - 1.6688(\sin\lambda + f_{sf} \cos\lambda) f_{rf}} \quad (25)$$

F_r can be calculated for all the other values are known. With F_r determined, $R_3 + R_4$ can be calculated from Equation 23.

It is now possible to compute the power required to overcome sliding and reciprocating friction during normal pump operation for desired inlet vacuums and pump speeds since the coefficients of friction and the necessary normal

forces have been determined.

$$(P_{sf})_n = \frac{4\ f_{sf}\ F_r\ V}{550} \qquad (26)$$

$$(P_{rf})_n = \frac{4\ f_{rf}\ (R_3 + R_4)\ V_r}{550} \qquad (27)$$

III. RESULTS

Figures XI, XII, XIII, and XIV are faired curves of the data for Experiments 1, 2, 3, and 4, respectively. Fairing of the data curves was performed on large scale graphs using the arithmetical mean of the recorded data to determine the faired curve.

Figures XV and XVI are curves of calculated values of f_{sf}, f_{rf}, P_{sfd}, P_{rfd}, P_{sf}, and P_{rf} which were computed by the procedure outlined previously. These curves are drawn from the data listed in Tables IX and X.

Figures XVII and XVIII are curves which represent the calculated values of the friction power and their relationship to the total power as measured in Experiment 3. These curves show one of the major objectives of this thesis; i.e., the proportion of power required to overcome friction to the total power required.

The results of Experiment 5 will be given in the form of several observations. This is required by the fact that this experiment was only a partial success in measuring the temperature at the sliding surface. The temperature measured was far less than the surface temperature as predicted using Archard's formulation. This was due to our inability to locate a thermocouple close enough to the sliding surface. The strength of the vane material limited us in the location of the thermocouple; it was located about one-sixteenth of an inch from the sliding surface. The thermocouple of necessity had to be electrically insulated from the vane material which

introduced some thermal insulation. Due to these two restrictions and the low thermal conductivity of the vane material, it was not surprising that the temperature measured was lower than that predicted.

From the temperature recorded we can indicate the following trends. The surface temperature increases with an increase in the sliding velocity and in the normal force at the point of contact of the sliding surfaces. The change in surface temperature is small for large changes in sliding velocity and normal force. At a constant speed the torque measured on the force scale remained essentially constant as the vane temperature increased from the ambient temperature to a quasi-steady-state temperature. The increase in vane temperature was approximately 50 Farenheit degrees during a continuous operation at constant speed of two hours duration.

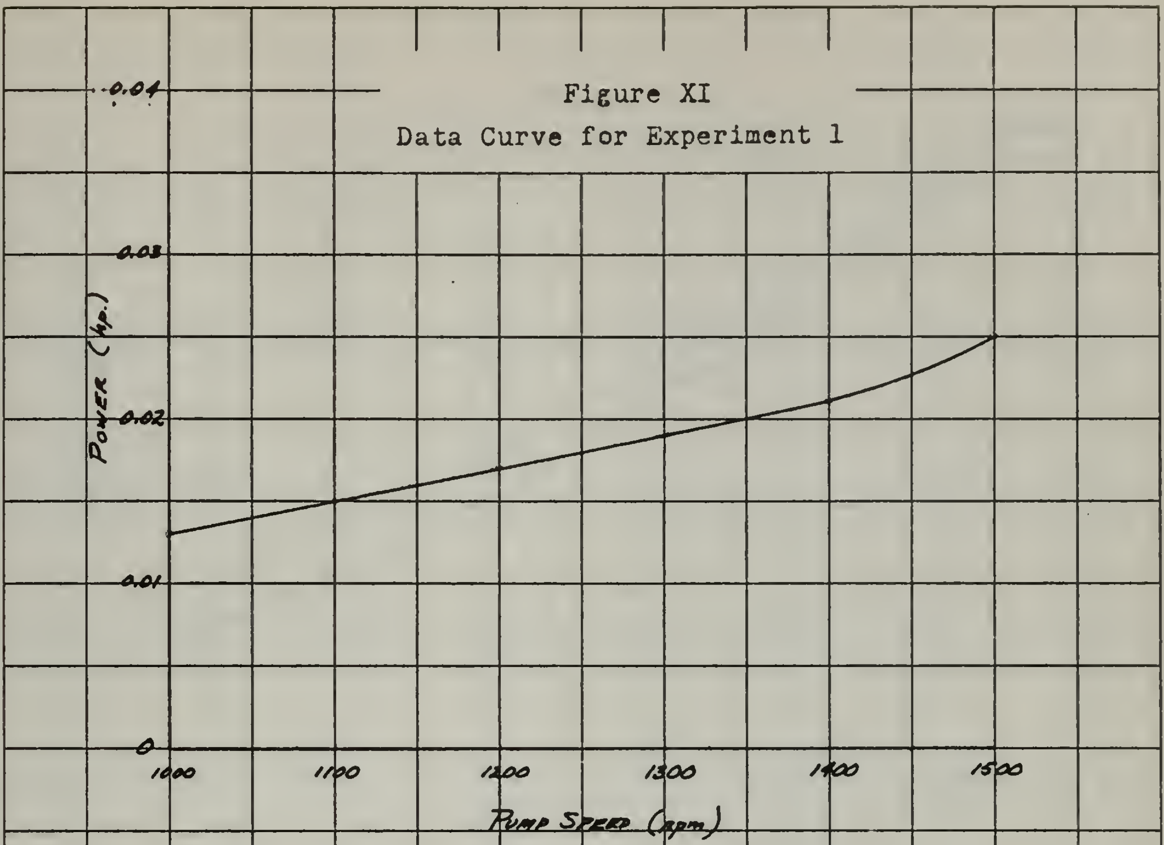

Figure XI
Data Curve for Experiment 1

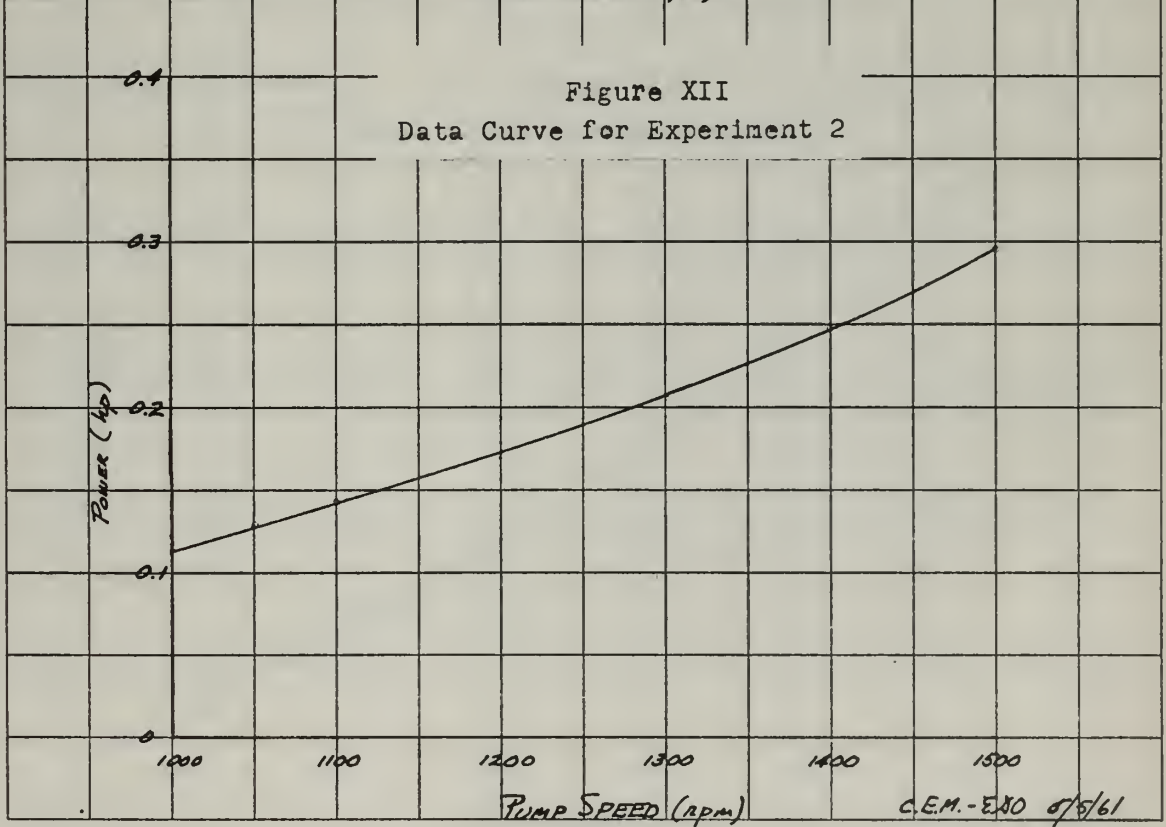

Figure XII
Data Curve for Experiment 2

Figure XIII

Data Curve for Experiment 3

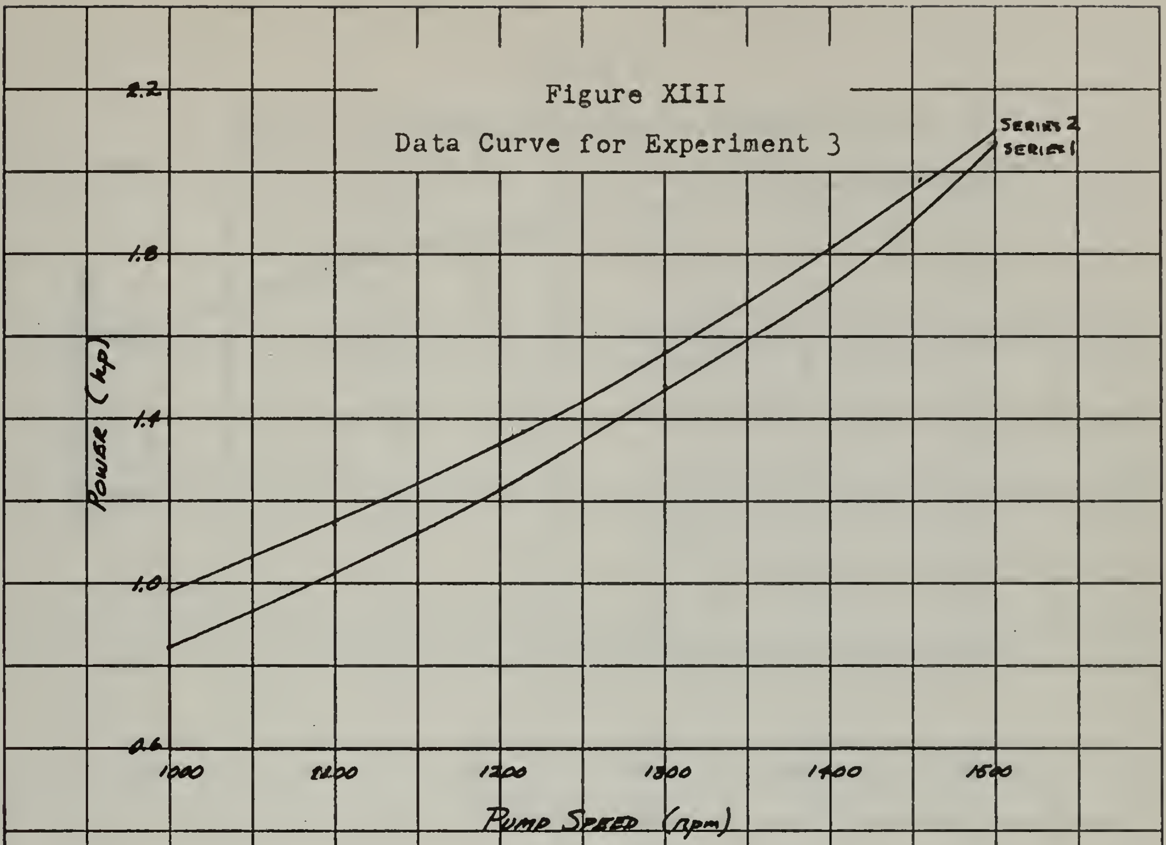

Figure XIV

Data Curve for Experiment 4

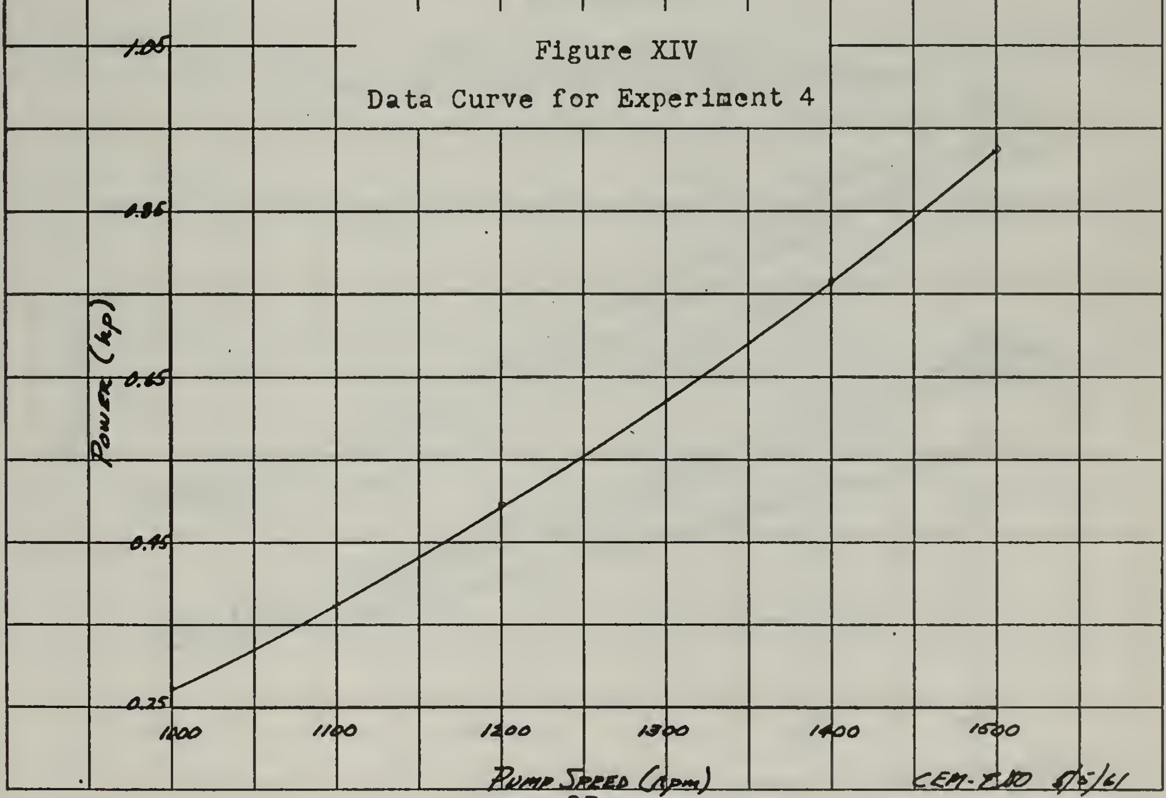

Figure XV

Curves of Calculated Friction Coefficients

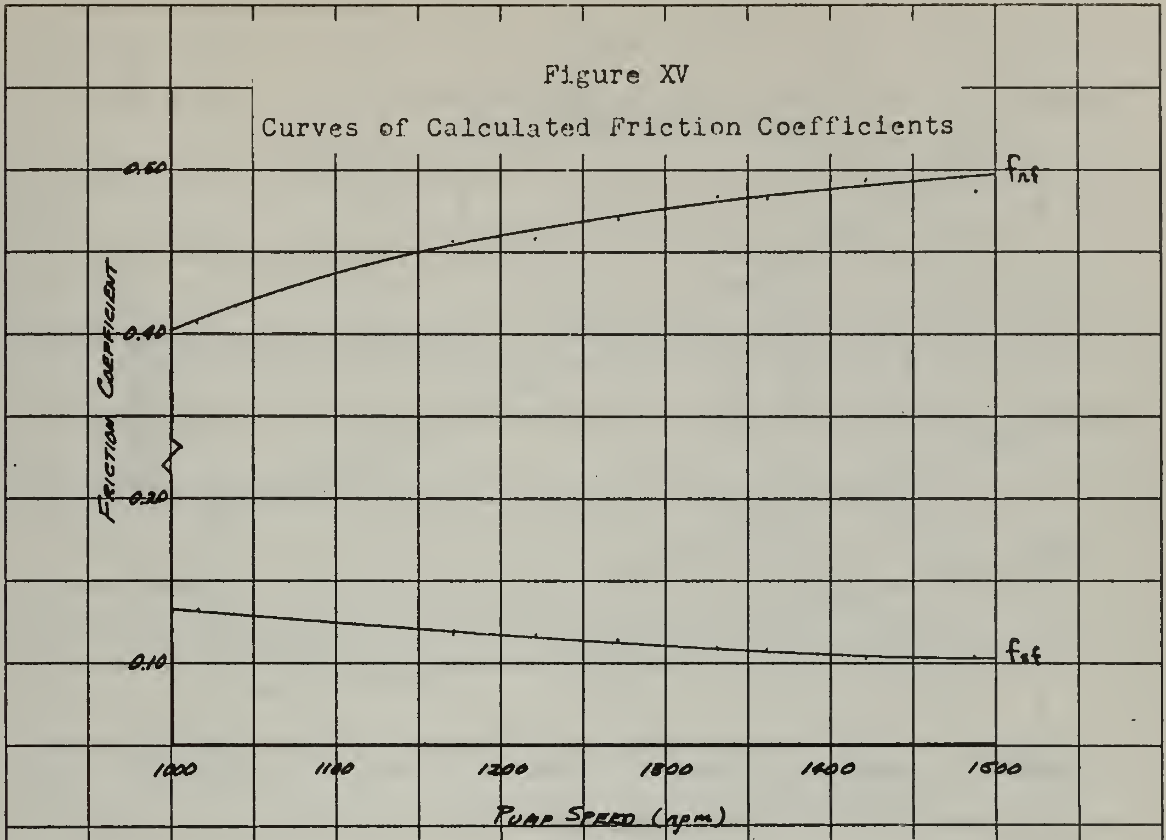

Figure XVI

Curves of Calculated
Sliding and Reciprocating Friction Power

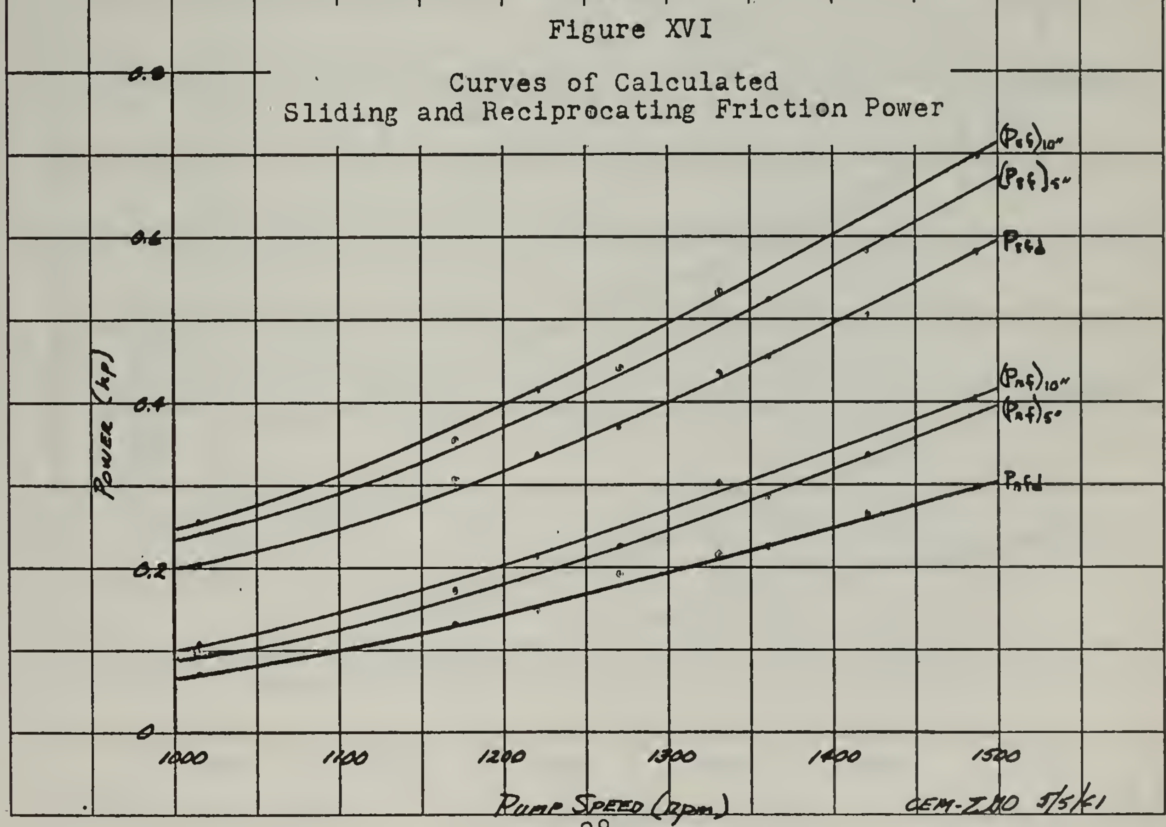

CEM-I 110 5/5/61

Figure XVII

Distribution of Friction Power for 5" Hg Inlet Vacuum

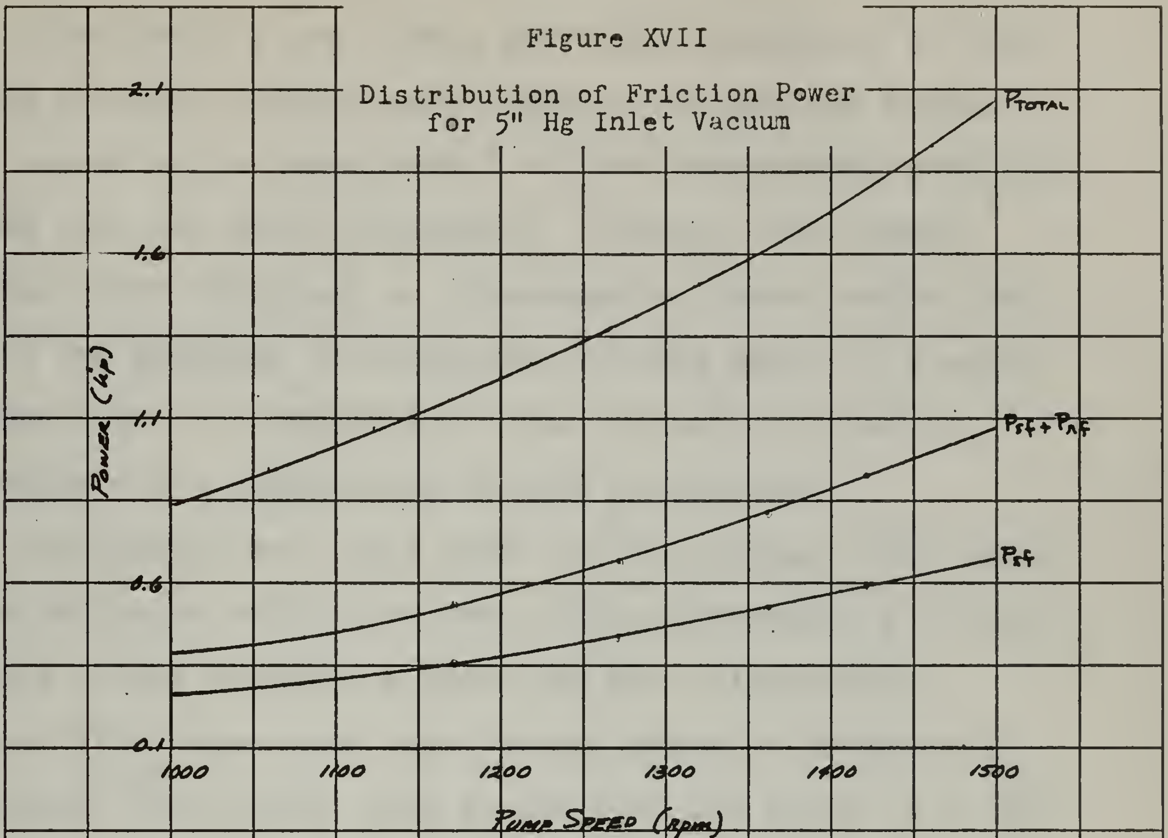

Figure XVIII

Distribution of Friction Power for 10" Hg Inlet Vacuum

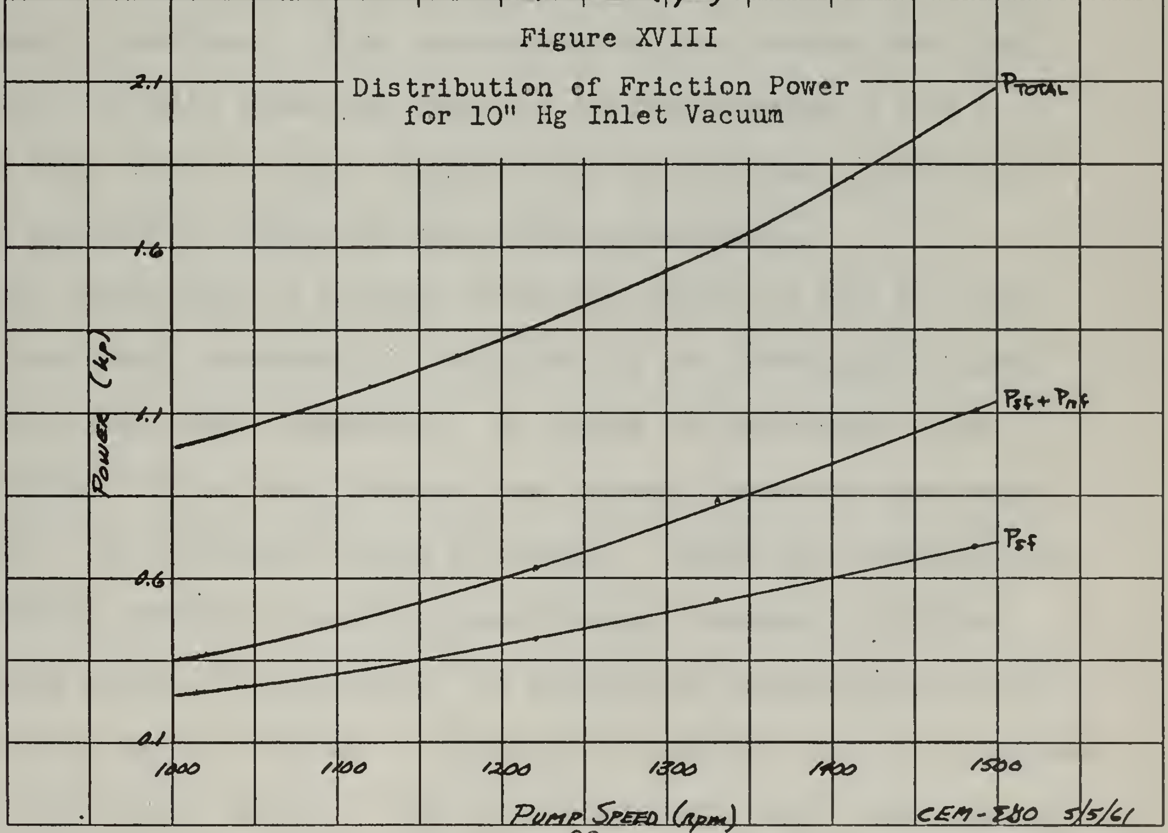

CEM-880 5/5/61

IV. DISCUSSION OF RESULTS

Experiments 2 and 5 were performed separately to note if any pressure effects were present when the end plates were closed as in Experiment 2 -- both experiments were performed with the rotor concentric. However, both power readings were identical at corresponding speeds which dispelled any thoughts that pressure effects might be present in Experiment 2. Experiment 5 was further utilized to investigate the temperature effects on friction.

Photographs were also taken of the pressure-time cyclic characteristics within the pump during Experiment 4 to note whether or not pressure effects had been eliminated. Figure XXVIII does show that the influence of pressure is negligible for various pump speeds when the rotor is in the eccentric position. This corroborated the notion that the pressure effects were not present in Experiments 2 and 5 since they will be more significant, if present, with the rotor eccentric than with the rotor concentric.

By referring to Figures XVII and XVIII it can be seen that the power consumed by friction is an appreciable part of the total power required. As speed is increased, the centrifugal force and, hence, the normal force of the vane against the cylinder casing increase. Since the coefficient of sliding friction remains essentially constant, sliding friction power from Equation 26 increases exponentially with increasing speed because V increases linearly and F_r increases in a non-linear manner. The same arguments also explain why

the reciprocating friction power increases in a similar fashion because V_r increases linearly with speed and $R_3 + R_4$ like F_r increases in a non-linear manner.

This explains partially why the percentage of total power consumed by friction steadily increases with speed. The percentages represented by Figure XIX are rather high even for this low speed range of 1000 to 1500 rpm. Friction, therefore, limits the rotary sliding vane machine to relatively low speeds.

Now note the effect caused by increasing the pressure differential across the vanes at a constant speed. Equation 25 shows that the normal force F_r against the cylinder casing is a function only of the pressure force H_p at a constant speed. Figure XVI shows that the sliding friction power increases with an increase in H_p, assuming that f_{sf} stays constant at the same pump speed. The reaction forces R_3 and R_4 also increase when a greater pressure differential is applied to the exposed portion of the vane, which results in an increased reciprocating friction power dissipation at a given speed as H_p increases. Increased pressure differential, like increased speed, causes the percentage of friction power to increase.

Next, consider the values of the sliding and reciprocating coefficients of friction. Figure XV shows a slight decrease in the sliding friction coefficient with an increase in speed. From Mordike[12] the coefficient of friction of graphite on iron is seen to remain essentially constant up to 500° Centigrade. Observations from Experiment 5 show that

Figure XIX

Percentage of Friction Power

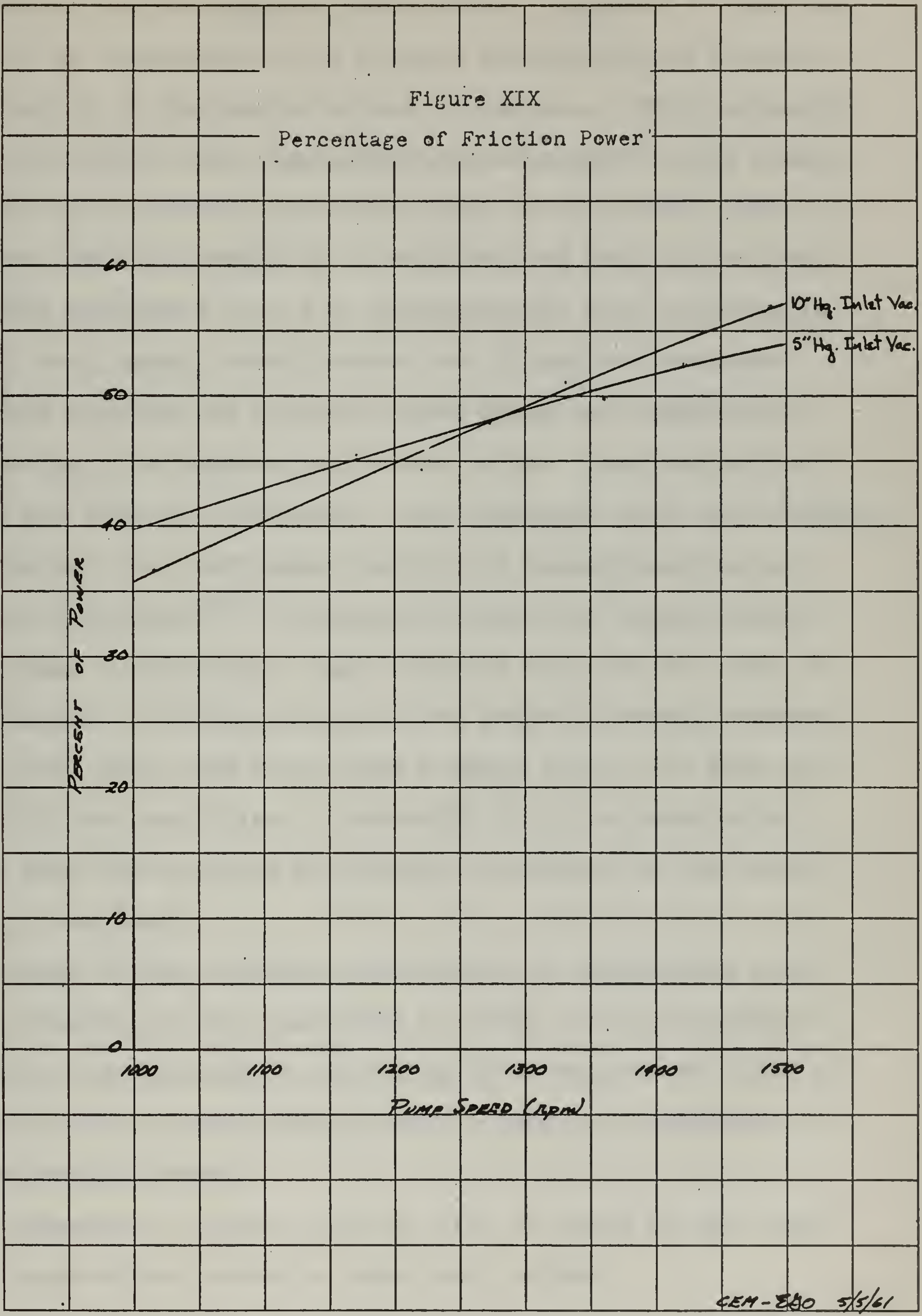

the contact or surface temperature at the vane and casing interface does not approach this value. Archard[1] has formulated an expression for a sliding coefficient of friction for similar or dissimilar metals in contact. This expression varies directly with temperature and inversely as the square root of the speed and the fourth root of the normal load. However, from Experiment 5 it was observed that as the temperature increased due to an instantaneous step increase in speed, and, hence, normal force, the friction horsepower remained constant at this new speed while the temperature was rising to a quasi-steady-state value. Considering that speed and load were constant, this indicates that the friction coefficient is a very weak function of temperature, as depicted by Mordike[12]. Noting also that the normal force, I_{cd}, poses a relatively light reaction force on the vane in the concentric configuration in the range of speeds studied, it is felt that load would have a minor effect, if any, on the friction coefficient. Archard[1], it has been noted, found that the variance was related inversely to the fourth root of the load.

Based on the preceding discussion of temperature and load effects, we felt justified in using the same sliding friction coefficients as determined from Experiment 2 for an analysis of the pump during normal eccentric operation at corresponding speeds.

Therefore, sliding friction will be taken to vary only with speed--this variation being only slight.

The reciprocating friction coefficient, f_{rf}, is more

than four times the sliding friction coefficient. First, the discussion on temperature effects as related to sliding friction will be taken as valid for the reciprocating friction. Experiment 4 which included both sliding and reciprocating friction effects showed no increase or decrease in friction power as the temperature was allowed to reach a quasi-steady-state. Further discussion will be made in reference to load considerations.

An explanation of the relatively high reciprocating friction coefficient is now in order. Twice a revolution the vanes must overcome a static coefficient of friction which, of course, will be higher than the sliding coefficient of friction. The reciprocating friction coefficient as we have defined it, therefore, embraces both static and dynamic considerations.

At this point as explanation should be made regarding the summation of forces along the vane as shown in Equations 10 and 23. Question may arise about the sign of the quantities $f_{rf}(R_1+R_2)$ and $f_{rf}(R_3+R_4)$ since they have different signs in the converging and diverging portions of the cycle due to the change in direction of motion of the vane. However, since this cycle analysis is based upon average values, the average value of the total acceleration has been used. This average acceleration is always directed toward the rotor center and the component along the vane is always directed into the vane slot. Therefore, with this concept the vane motion is on the average always into the vane slots which, in turn, suggests that the friction forces $f_{rf}(R_1+R_2)$ and

$f_{rf}(R_3+R_4)$ must always oppose this motion. Choosing this sign convention constitutes dictating a definition for f_{rf} and, hence, f_{rf} is only valid as we have defined it. The relations given by Equations 10 and 23 are necessary to permit the system of equations developed in the Procedure to have a determinate solution.

It will be noted that the reciprocating friction coefficient as plotted in Figure XV increases slightly with speed--the converse of the sliding friction coefficient behavior. Equation 22 defines f_{rf}; inspection of Equation 18 shows $f_{rf}(R_1+R_2)$ to be dependent on the sliding friction coefficient. Therefore, a rather complicated relationship does exist between f_{sf} and f_{rf} within their definition such that as f_{sf} decreases slightly, f_{rf} rises slightly with an increase in pump speed.

Now for further mention of the reaction load $R_3 + R_4$ upon which reciprocating friction power is based. Again the load is relatively small and any variation in it will have negligible effect on the reciprocating friction coefficient. However, from Equation 24 one notes that $R_3 + R_4$ is a weak function of f_{sf}. We can, for practical purposes, say that the reciprocating and sliding friction effects can be separated from one another. Nevertheless, we must be mindful that there is a relationship between the two.

The coefficients of sliding friction determined experimentally are reasonable when compared with quoted values for carbon graphite sliding on cast iron. With the advent of new materials with low frictional characteristics such as

polytetrafluoroethylene, one might predict that the future of dry rotary sliding vane machinery will be brighter.

Suppose for this same pump that all factors remain constant except the coefficient of sliding friction and the coefficient of reciprocating friction. Suppose that we choose as the vane material an exotic material which has a sliding friction coefficient of 0.05 when the pump speed is 1170 rpm.

The purpose of the following calculations will be to determine the reduction in friction power, if any, when the pump is operating with an inlet vacuum of 5 inches of mercury.

An assumption must be made for a reciprocating friction coefficient. It is reasonable to assume that f_{rf} will be about five times greater than f_{sf}; hence, f_{rf} is assumed to be 0.25. This value may be rather high in light of our experimental results--specifically at 1170 rpm and 5 in. Hg.

$$\frac{f_{rf}}{f_{sf}} = \frac{0.4561}{0.1183} = 3.85$$

The following quantities do not change with varying friction coefficients.

F_a = 5.631 lbs.

H_p = 1.199 lbs.

H_c = 6.145 lbs.

V = 23.313 ft./sec.

V_r = 2.847 ft./sec.

From Equation 25

$$F_r = \frac{F_a + 1.3344\ f_{rf}H_p - 0.3344\ f_{rf}H_c}{(\cos\lambda - f_{sf}\ \sin\lambda) - 1.6688(\sin\lambda + f_{sf}\ \cos\lambda)f_{rf}}$$

$$= \frac{5.63+1.3344(.25)(1.199)-0.3344(.25)(6.145)}{[.848-.05(.5299)]-1.6688[.5299+.05(.848)](.25)}$$

F_r = 9.46 lbs.

From Equation 24

$$R_3+R_4 = 1.6688(\sin\lambda+f_{sf}\ \cos\lambda)F_r+1.3344H_p-.3344\ H_c$$

$$= 1.6688[.5299+.05(.848)]\ 9.46+1.3344(1.199)-(.3344)6.145$$

R_3+R_4 = 8.58 lbs.

From Equation 26

$$P_{sf} = \frac{4f_{sf}F_rV}{550}$$

$$= \frac{4(.05)(9.46)(23.313)}{550}$$

P_{sf} = 0.080 hp.

From Equation 27

$$P_{rf} = \frac{4f_{rf}(R_3+R_4)V_r}{550}$$

$$= \frac{4(0.25)(8.58)(2.847)}{550}$$

P_{rf} = 0.044 hp.

These calculations have been based upon a sliding friction factor which has been reduced by a factor of 2.37. The reciprocating friction factor has been reduced only by a factor of 1.825.

Nevertheless, sliding friction power has been reduced by a factor of 4.45. The reciprocating friction power has been reduced by a factor of 3.89. Total percentage reduction

in friction power is

$$\frac{(.5275 - .1242)}{.5275} \times 100 = 76.4\ \%$$

Based upon the assumptions stated for this friction power comparison, one should further investigate the seemingly positive qualities of low friction materials. Since power dissipation by friction is much less, there is less preheating of the working fluid which, in turn, reduces pumping irreversibilities.

Perhaps the effect of changing the angle between the rotor radius and the vane slots, α, will have a significant effect on frictional considerations. An analysis will now be attempted using the same pump configuration with only the angle α altered to a value of zero degrees. All quantities will remain constant except those influenced by this angle change. Frictional coefficients used will be those determined from our experimental work.

Again a speed of N = 1170 rpm. will be used.

$f_{sf} = 0.1183$

$f_{rf} = 0.4561$ (Use this value even though V_r has changed slightly.)

Referring to Figure VIII

If $\alpha = 0$

then $\beta = 0$

$\lambda = 0$

From the pump geometry since

$R_v = 2.282''$ and $e = 0.3715''$ as before

$$R_{g_{new}} = R_v - \left(\frac{R_v - R_g}{\cos \alpha}\right)$$

$$= 2.282 - \frac{2.282 - 1.6325}{\cos 38^{\circ}}$$

$R_{g_{new}} = 1.457''$

Eqn.(11) $F_a = \frac{w}{g} (\frac{2\pi N}{60})^2 \frac{R_{gn}}{12} \cos\beta$

$$= \frac{0.131}{32.2} (\frac{2\pi}{60})^2 (1170)^2 (\frac{1.457}{12})(1)$$

$F_a = 7.42$ lbs.

Eqn. (16) $V_r = \frac{N\ e \sec\lambda}{180}$

$$V_r = \frac{(1170)(.3715)\ 1}{180}$$

$V_r = 2.415$ ft/sec. vs. 2.847 ft/sec. for original case.

A refinement could be made on f_{rf} based on this new value of V_r but f_{rf} changes little with V_r.

$H_p = \frac{h\ l\ \Delta\ P_{ave}}{4}$ (again using 5" Hg. inlet vacuum)

$h_{new} = h \cos\alpha$

$= (0.4229) \cos 38°$

$h_{new} = 0.333$

$H_{p_{new}} = 0.944$ lbs.

Eqn. (21) $H_c = \frac{w}{g} (\frac{2\pi N}{60})^2 \sin\beta$

$H_c = 0$

Referring to Figure XXIV we can make a new vane reaction analysis where the distance between R_3 and R_4 is now 1.3546", and the distance between R_4 and H_p is now 0.1665". By summing moments $R_3 + R_4 = 1.245H_p + 1.491F_r f_{sf}$.

Substituting (R_3+R_4) in the expression for F_a

$$F_a = F_r - f_{rf}\ (1.245H_p + 1.491\ F_r f_{sf})$$

Solving for F_r:

$$F_r = \frac{F_a + 1.245\ f_{rf}\ H_p}{1 - 1.491\ f_{rf}\ f_{sf}}$$

Substituting values

$$F_r = \frac{7.42 + 1.245(.4561)(.944)}{1 - 1.491(.4561)(.1183)}$$

$$F_r = 8.66\ \text{lbs.}$$

Solving for $R_3 + R_4$

$$(R_3+R_4) = 1.245(.944)+1.491(8.66)(.1183)$$

$$(R_3+R_4) = 2.705\ \text{lbs.}$$

Now to calculate power dissipated.

Eqn. (26) $$P_{sf} = \frac{4f_{sf}\ F_r\ V}{550}$$

$$P_{sf} = \frac{4(.1183)(8.66)(23.313)}{550}$$

$$P_{sf} = 0.174\ \text{hp.}$$

Eqn. (27) $$P_{rf} = \frac{4f_{rf}(R_3+R_4)V_r}{550}$$

$$= \frac{4(.4561)(2.705)(2.415)}{550}$$

$$P_{rf} = 0.0216\ \text{hp}$$

From these calculations one notes that the reciprocating friction has been reduced to a negligible value. The sliding friction power has been reduced to approximately half its original value. Percentage reduction in total friction power is

$$\frac{(.5275 - .1956)}{.5275} \times 100 = \underline{62.9\ \%}$$

These calculations show that a change in the angle of the vane from the radial position can have a significant effect on frictional power consumed. Any reduction of α from 38° will decrease the friction power with the maximum reduction in friction power occurring when $\alpha = 0$. Apparently, the only reason for canting the vanes at an angle is to permit a greater vane width to be housed in the rotor. This, of course, will allow a greater eccentricity and, hence, a greater capacity.

V. CONCLUSIONS AND RECOMMENDATIONS

Power dissipated by friction is an appreciable fraction of the total power necessary to run a "dry" rotary sliding vane machine. Sliding and reciprocating friction as defined in this paper each represent a significant portion of the total power input. An increase in the pressure force and an increase in the speed each raise the power dissipated by the two modes of friction. As a result of the total friction power increasing exponentially with speed and pressure, the "dry" rotary sliding vane machine is restricted to operation in a relatively low speed range.

Temperature effects were negligible for this configuration of carbon graphite sliding on cast iron; however, temperature is a factor which always must be considered--particularly when temperature-sensitive materials are used.

The variation in normal force between vane and casing showed no significant effect on friction coefficients for the relatively light forces involved. Nevertheless, the effect of heavier loads which may also involve plastic and/or elastic deformations of the materials in contact must be considered, as this will affect the coefficients of friction.

Factors which may reduce the friction power significantly are new low friction vane materials and placement of the vanes in radial slots within the rotor. Comparative calculations with the experimental design show that these two considerations do reduce friction power by a considerable fraction. Hopefully, an actual design incorporating either

[illegible]

[illegible]

[illegible]

[illegible]

[illegible]

or both low friction vanes in radial slots would approach theoretical predictions. Only an experimental analysis will determine the actual reduction.

An increase in temperature caused by friction further raises the temperature of the working fluid as it passes through the pump cycle. More irreversibility in compression is introduced and, hence, more work is required to overcome the effects of this temperature increment. Introducing a friction power reduction will, therefore, decrease the amount of irreversibility.

Strength considerations of the vane material are also important. Slight misalignment, shock or a relatively small departure from a specified narrow speed and pressure operating range are all detrimental to the carbon graphite vane. The search for new vane materials must, necessarily, account for these factors.

The investigation of friction phenomena requires an experimental analysis. This technique is the only valid procedure for determining usable theoretical formulations which include the existing design parameters of a given device. Using these theoretical formulations, one can then predict the effects of changes in design parameters. These predictions will indicate trends for the improvement of the original design. The actual effects of changes in design parameters can only be found by further experimentation which will prove or disprove these predictions.

VI. APPENDIX

APPENDIX A

Details of Procedure

A.1 Procedure for Determining R_v, h, R_g, β, and λ.

When the pump rotor is in the eccentric position and rotating, R_v, h, R_g, β, λ, and H_p all vary as the angular position of the rotor changes. The power dissipated during normal pump operation actually varies as the angular position of the rotor changes. In our experiments the power measured is an average power which is independent of rotor position. In effect, then, the power measured is the power that would be dissipated if all the varying quantities were held constant at their average values.

To find the average of R_v, h, R_g, β, and λ, a drawing of the rotor and cylinder bore was made. (Figure XX). Rotor positions were indicated for every 15 degrees of rotation, and the vanes were drawn in at an angle of 38 degrees to the rotor radius at each position. The R_v, h, and R_g values were then measured for each rotor position. These values are tabulated in Table V. The averages were then found, and a large scale drawing similar to Figure VIII was made using these average values, the rotor radius, the angle α, and the vane width. These dimensions fixed the angles β and λ at their average values which were then measured.

Figure XX

Rotor Layout for R_g, h, R_v, β Average Values

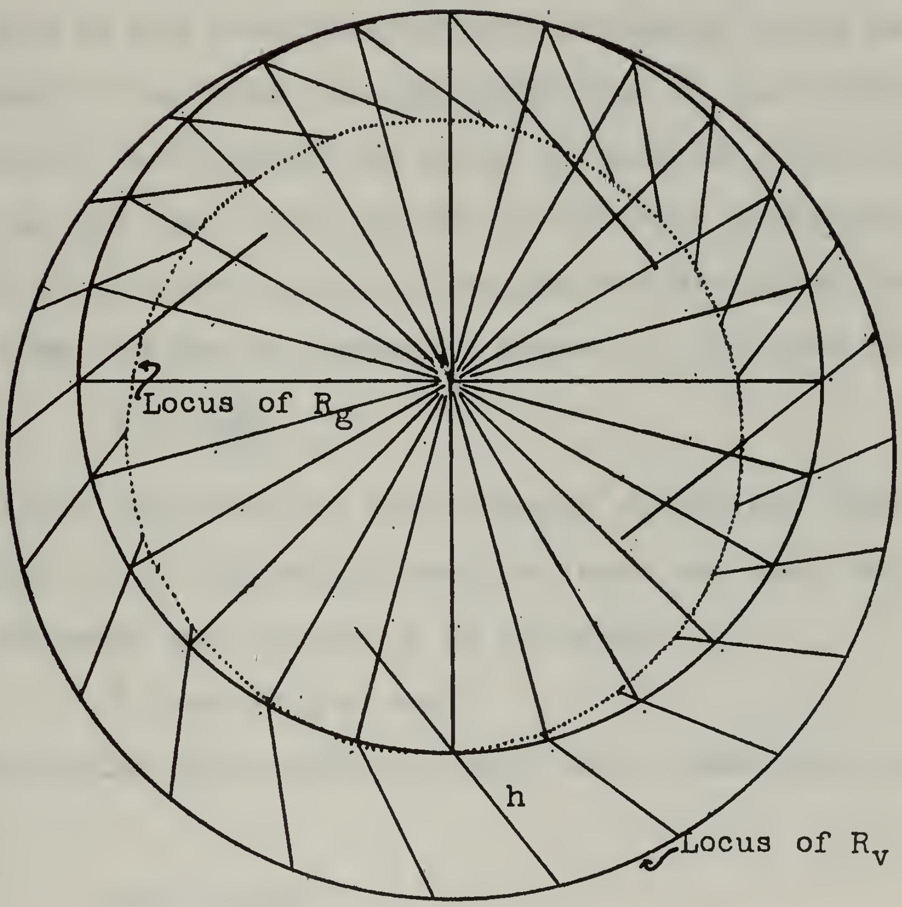

[illegible]

A.2 Resolution of the Total Vane Acceleration with Rotor Eccentric.

When the rotor is mounted in the eccentric position, the vane experiences three accelerations--the centripetal acceleration, the acceleration into and out of the vane slot, and a Coriolis acceleration. The total acceleration is the vector sum of these three accelerations. To determine the forces due to the total acceleration resolved along the vane and normal to the vane, we are interested in the components of the total acceleration in these directions. The acceleration of the vane into and out of the vane slots acts in opposite directions in the converging and diverging sections of the pump and has no component normal to the vane. (Figure XXI).

$$a_p = \frac{d^2x}{dt^2} \tag{28}$$

The Coriolis acceleration also changes direction from the converging to the diverging section since the vane reciprocating velocity and, hence, u is reversed.

$$2\, u\omega = 2\, V_r\, \omega \cos \beta \tag{29}$$

The centripetal acceleration always acts toward the rotor center.

$$a_m = r_{cg}\omega^2 \tag{30}$$

The magnitudes of these three accelerations has an average value which is nearly equal for the converging and diverging sections of the pump and depends on the average values of R_g and V_r. To find the average total acceleration acting during one revolution at a given speed, it is necessary to average the total acceleration in the converging section

Figure XXI

Rotor Layout for Total Acceleration Resolution

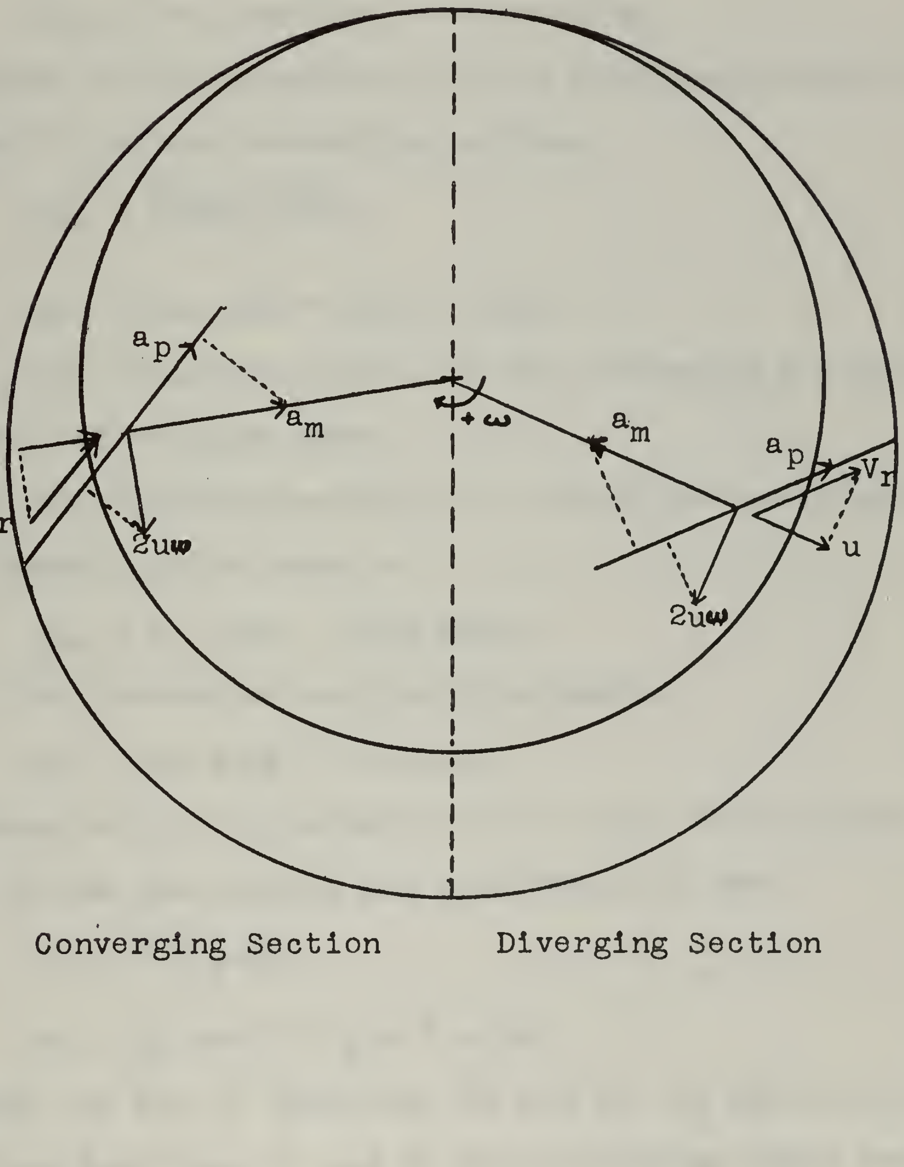

Converging Section Diverging Section

[illegible]

[illegible]

and the total acceleration in the diverging section. For our purposes, we may average the components of the three accelerations in the two sections normal to and along the vane.

For the diverging section the sum of the components acting along the vane is

$$a_{avd} = a_m \cos\beta - a_p + 2\,u\omega\sin\beta \tag{31}$$

and for the converging section this sum is

$$a_{avc} = a_m \cos\beta + a_p - 2\,u\omega\sin\beta \tag{32}$$

The average of the components of the total acceleration along the vane during one revolution is then

$$a_{av} = \frac{a_{avd} + a_{avc}}{2} \tag{33}$$

$$a_{av} = a_m \cos\beta = R_g\,\omega^2 \cos\beta \tag{34}$$

Since a_p and $2u\,\omega\sin\beta$ cancel in this averaging process, they need not be calculated.

For the diverging section the sum of the components acting normal to the vane is

$$a_{nd} = a_m \sin\beta - 2u\,\omega\sin\beta \tag{35}$$

and for the converging section this sum is

$$a_{nc} = a_m \sin\beta + 2u\,\omega\sin\beta \tag{36}$$

The average of the components of the total acceleration normal to the vane during one revolution is then

$$a_n = \frac{a_{nd} + a_{nc}}{2} \tag{37}$$

$$a_n = a_m \sin\beta = R_g\,\omega^2 \sin\beta \tag{38}$$

With the aid of Equations 34 and 38, F_a and H_c can be found from Equations 11 and 21 by multiplying these average accelerations by the mass of one vane.

A.3 Derivation of Equation 19 for ($R_1 + R_2$)

The use of a free body diagram of the vane is necessary to compute R_1 and R_2. The values of R_1 and R_2 are varying quantities which are dependent on the angular position of the rotor. Although the magnitudes of R_1 and R_2 vary with rotor position, the direction of action is always that as shown in Figures IX and XXII. This initially was an assumption, but actual calculations as well as the appearance of the vanes after running Experiment 4 confirmed this assumption. The vanes showed signs of wear which could only be explained by having R_1 and R_2 act as shown. The average values of R_1 and R_2 for one revolution at a given speed are found by using the average values of H_c, F_{rd}, and h in the free body diagram. Since R_1 and R_2 always act in the directions shown for the speeds used in this experiment, the equation for the sum of the average values will always appear in the same form.

Figure XXII

Vane Free Body Diagram

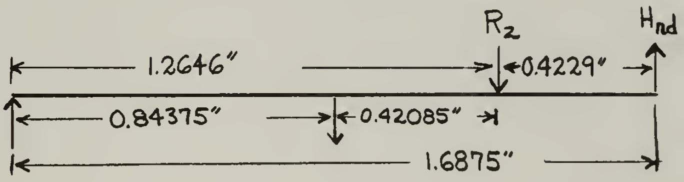

From Figure XXII we can solve for R_1 and R_2 by summing the moments of the forces. Summing the moments about R_1 we have:

$$0.84375\ H_c + 1.2646\ R_2 - 1.6875\ H_{rd} = 0 \tag{39}$$

Solving for R_2:

$$R_2 = \frac{1.6875H_{rd} - 0.84375H_c}{1.2646} \tag{40}$$

Summing the moments about R_2 we have:

$$1.2646R_1 - 0.42085H_c - 0.4229H_{rd} = 0 \tag{41}$$

Solving for R_1:

$$R_1 = \frac{0.42085H_c + 0.4229H_{rd}}{1.2646} \tag{42}$$

Adding Equations 40 and 42:

$$R_1 + R_2 = \frac{2.1104H_{rd} - 0.4229H_c}{1.2646} \tag{43}$$

or:

$$R_1 + R_2 = 1.6688H_{rd} - 0.3344H_c \tag{19}$$

A.4 Analysis of the Scope Presentations from Experiment 3 to Determine the Average Pressure Force Across a Vane

The pressure force which acts across a vane is a quantity which depends on the angular position of the rotor since the pressure differential across a vane and the vane area on which the pressure differential acts are both varying quantities. The pressure differential across a vane is also dependent on the rotor speed and the inlet vacuum. The determination of the pressure force can only be made at those speeds for which photographs of the scope presentations were obtained. The pictures were taken at random intervals over the speed range. Four pictures were taken for each of the two inlet vacuums investigated.

In order to use the data presented on the scope, the scope presentation of the pressure transducer output had to be related to the angular position of the rotor.

Several methods were tried to relate the presentation to rotor position. The inlet vacuum was varied to observe any changes in the scope presentation. The method resulted in fixing point a' on Figure XXIIIa in the vicinity of the inlet port of Figure XXIIIb. However, this correspondence was not sufficiently accurate for our purposes.

It was decided that point b on Figure XXIIIa should occur in the vicinity of the exhaust port on Figure XXIIIb. A large scale drawing similar to Figure XXIIIb was made with the rotor free to rotate. A rotor reference position was chosen near the exhaust port corresponding to point b. The rotor position was then changed in increments of angular

Figure XXIII

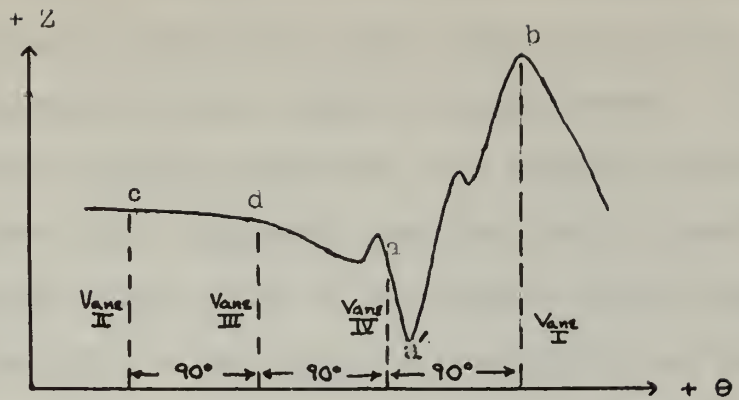

(a)

Typical Cycle Pressure-Time Characteristic

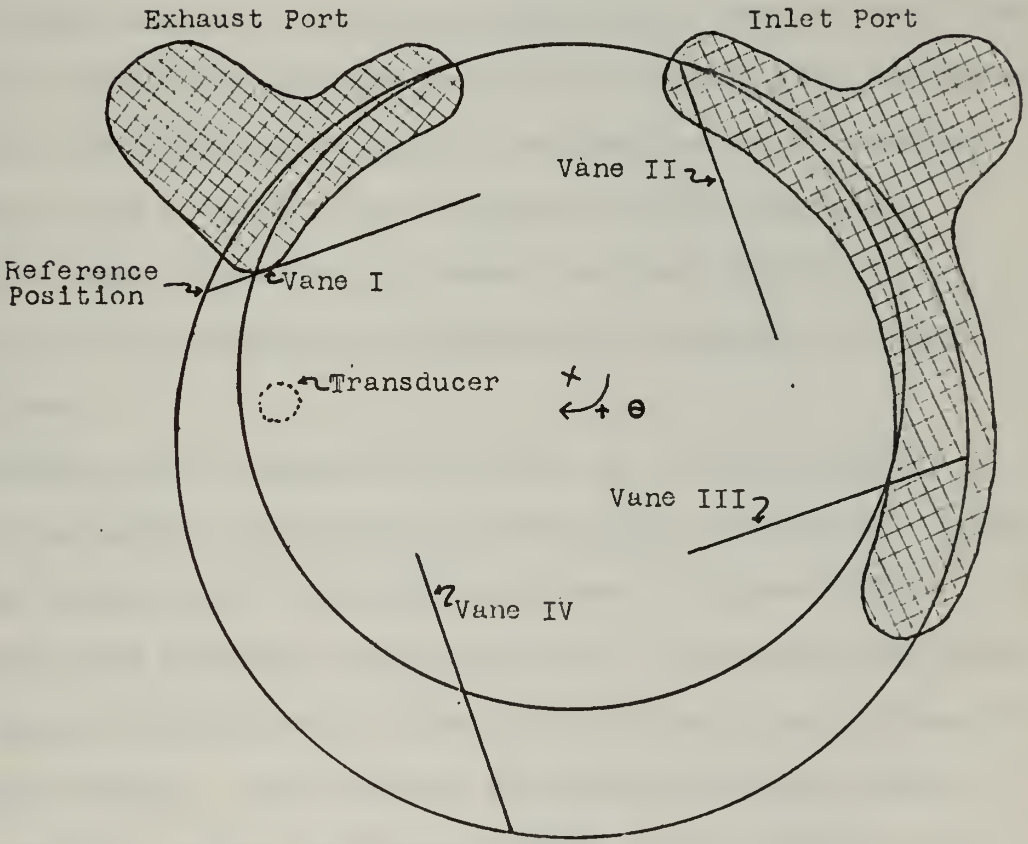

(b)

Rotor Layout for Pressure Analysis

displacement, and the pressure variations shown on the scope presentation were noted. Since the scope presentation was adjusted to be eighteen horizontal units wide, one unit is equal to twenty degrees of rotor angular displacement. For each rotor reference position selected, the pressure variation was checked to insure that variation was physically possible as the volume between Vanes I and II on Figure XXIIIb changed. By this process the point b was fixed as accurately as possible corresponding to the reference position for Vane I which is just prior to Vane I exposing the exhaust port as shown on Figure XXIIIb. This reference position was checked using each picture of the pressure variation and was found to fit each pressure variation presentation more closely than any other reference position. It is felt that this reference position corresponding to point b as determined is accurate to within plus or minus five degrees of rotor position. Since the scope presentation cannot be read within an accuracy of five degrees, the reference position is assumed to be fixed.

Knowing this reference position, it is now possible to find the pressure differential across each of the four vanes when the rotor is in the position shown in Figure XXIIIb. If the rotor were advanced ninety degrees, the transducer output would cause the deflection shown for the position of Vane II on Figure XXIIIa. The pressure differential across Vane I in the position shown on Figure XXIIIb is the vertical difference, in inches, between points b and c on Figure XXIIIa multiplied by the scope scale factor to convert inches of

scope deflection to volts of transducer output--the output voltage then being converted to pressure in pounds per square inch by entering the transducer calibration curve. (Figure XXIX). The transducer calibration curve information was supplied by the transducer manufacturer, Gulton Industries. The pressure force acting normal to Vane I is found by measuring the vane's exposure and multiplying this exposure by the vane length and by the pressure differential.

The pressure force acting normal to each of the vanes is found by repeating the above procedure. Referring to Figure XXIIIa, the procedure can be outlined by the following expressions:

$$\Delta p \text{ across Vane I} \sim (Z_b - Z_c)$$
$$\Delta p \text{ across Vane II} \sim (Z_c - Z_d)$$
$$\Delta p \text{ across Vane III} \sim (Z_d - Z_a)$$
$$\Delta p \text{ across Vane IV} \sim (Z_a - Z_b)$$

When the vertical deflection decreases, or the difference in the above expressions is positive in the direction of rotation, the pressure force is aiding the rotor rotation and is considered to be a negative force. The converse results in a force opposing rotation and is considered to be a positive force.

To find the pressure forces across each of the vanes during one revolution, the positions of a, b, c, and d are all moved to the right the same number of degrees and the rotor is rotated clockwise the same number of degrees. The vertical deflections and vane exposures are then measured for each of the vanes and converted to pressure forces. For

[illegible]

[illegible]

[illegible]

[illegible]

the purpose of this analysis nine rotor positions were used, which resulted in the computation of the pressure force across a single vane for one revolution at intervals of ten degrees of angular displacement of the rotor. The measured differences of scope deflections, in inches, are tabulated in Table VI. The pressure differences, vane areas, and the products of pressure difference times vane area are tabulated in Tables VII and VIII. The average effective force due to the pressure differential across one vane for one revolution of the pump rotor is computed from Tables VII and VIII. The average force, H_p, always acts to oppose the positive rotation of the rotor.

A.5 Derivation of Equation 24 for $(R_3 + R_4)$

A free body diagram is necessary to compute R_3 and R_4 just as the free body diagram was necessary for deriving Equation 19 for $(R_1 + R_2)$. Both R_3 and R_4 vary with rotor position but are assumed to act as shown in Figures X and XXIV. This assumption has been verified by the appearance of the vanes after running Experiment 3 and actual calculations for the range of operation considered. The average values of H_c, F_r, H_p, and h are used in the free body diagram. The use of the average pressure force, H_p, is probably not completely justified since H_p varies over a wide range of values; however, the torque measured by the dynamometer depends upon the average forces acting during one revolution of the pump rotor. Use of an average H_p is, therefore, the only means of accounting for the influence of the pressure differential across the vanes in this experimental procedure.

Although the pressure force is distributed over the exposed portion of the vane, it can be applied as a single force acting at the mid point of the exposed portion of the vane for the purposes of determining R_3 and R_4.

Figure XXIV

Vane Free Body Diagram

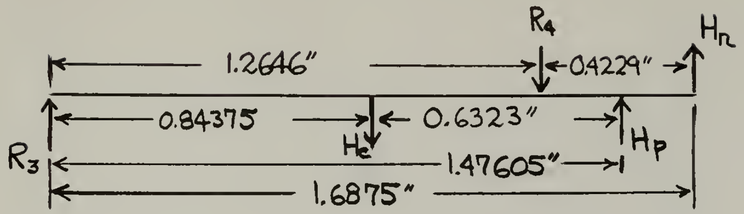

From Figure XXIV one can compute R_3 and R_4 by summing the moments of the forces. Summing the moments about R_3:

$$0.84375H_c + 1.2646R_4 - 1.47605H_p - 1.6875F_r(\sin\lambda + f_{sf}\cos\lambda) = 0 \tag{44}$$

Solving for R_4:

$$R_4 = \frac{1.6875F_r(\sin\lambda + f_{sf}\cos\lambda) + 1.47605H_p - 0.84375H_c}{1.2646} \tag{45}$$

Summing moments about R_4:

$$1.2646R_3 - 0.42085H_c - 0.21145H_p - 0.4229F_r(\sin\lambda + f_{sf}\cos\lambda) = 0 \tag{46}$$

Solving for R_3:

$$R_3 = \frac{0.4229F_r(\sin\lambda + f_{sf}\cos\lambda) + 0.21145H_p + 0.42085H_c}{1.2646} \tag{47}$$

Adding Equations 45 and 47 we have:

$$R_3 + R_4 = \frac{2.1104F_r(\sin\lambda + f_{sf}\cos\lambda) + 1.6875H_p - 0.4229H_c}{1.2646} \tag{48}$$

or

$$R_3 + R_4 = 1.6688F_r(\sin\lambda + f_{sf}\cos\lambda) + 1.3344H_p - 0.3344H_c \tag{24}$$

APPENDIX B

Summary of Data and Calculations

The data from Experiments 1, 2, 3, and 4 is listed in Tables I, II, III, and IV, respectively, in the order that it was obtained.

Table VI contains data taken from Figures XXVI and XXVII. Tables VII and VIII contain computed data based on the values of the measured deflections listed in Table VI.

Listed in Tables IX and X are the calculated values for the friction coefficients, the sliding friction power and the reciprocating friction power.

Figure XXV

Force Scale Calibration Curve

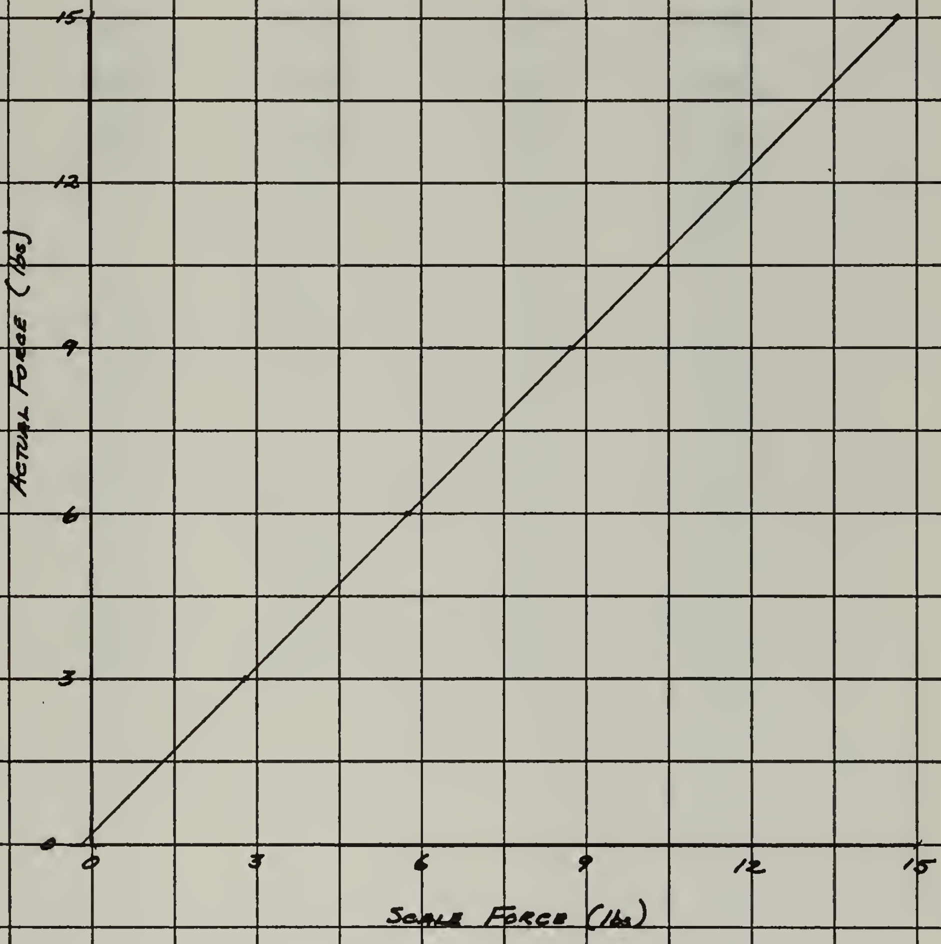

CEM-EDO 5/5/61

TABLE I

Data from Experiment 1

Speed (rpm)	Scale Force (lbs)	Actual Force (lbs)	Power (hp)
860	-0.05	0.13	0.013
975	-0.04	0.14	0.014
1125	-0.04	0.14	0.015
1340	0.00	0.17	0.020
1470	0.00	0.17	0.024
1630	0.05	0.23	0.036

TABLE II

Data from Experiment 2

Speed (rpm)	Scale Force (lbs)	Actual Force (lbs)	Power (hp)
990	1.15	1.34	0.126
1100	1.33	1.52	0.160
1275	1.77	1.96	0.238
1340	1.98	2.18	0.278
1425	2.32	2.52	0.342
1500	2.64	2.83	0.404
1130	1.38	1.56	0.168
1200	1.49	1.68	0.192
1235	1.56	1.75	0.206
1390	1.80	2.00	0.265
1500	2.00	2.20	0.314
1070	1.19	1.38	0.140
1205	1.34	1.53	0.176
1315	1.60	1.79	0.224
1410	1.73	1.94	0.260
1460	1.78	1.97	0.274
1050	1.06	1.25	0.125
1060	1.14	1.33	0.134
1250	1.38	1.57	0.187
1290	1.50	1.69	0.208
1360	1.58	1.78	0.231
1385	1.62	1.81	0.239
1150	1.17	1.36	0.149
1360	1.46	1.46	0.215
1515	1.82	2.01	0.290
1020	0.98	1.17	0.114
1230	1.20	1.39	0.163
1325	1.49	1.67	0.211
1485	1.71	1.90	0.269

[illegible]

[illegible]

[illegible]	[illegible]	[illegible]	[illegible]
[illegible]	[illegible]	[illegible]	[illegible]

TABLE III

Data from Experiment 3

Series 1 - Inlet Vacuum = 5" Hg

Speed (rpm)	Scale Force (lbs)	Actual Force (lbs)	Power (hp)
1010	8.70	9.00	0.865
1020	8.85	9.15	0.888
1030	8.75	9.07	0.889
1040	8.70	9.00	0.891
1134	8.30	8.60	0.928
1150	8.90	9.22	1.009
1165	10.70	11.05	1.226
1170	9.80	10.14	1.129
1184	10.10	10.44	1.177
1185	10.50	10.85	1.224
1260	10.95	11.30	1.355
1265	11.50	11.88	1.431
1270	11.90	12.29	1.486
1270	9.80	10.14	1.226
1300	11.70	12.07	1.494
1315	10.60	10.96	1.372
1325	12.40	12.78	1.612
1345	12.20	12.58	1.611
1360	12.00	12.35	1.599
1375	12.90	13.29	1.740
1420	13.90	14.30	1.933
1430	13.40	13.80	1.879
1440	13.00	13.39	1.836
1445	14.20	14.60	2.008
1450	14.00	14.42	1.991
1470	13.40	13.80	1.931
1478	14.40	14.81	2.080
1478	13.70	14.11	1.985
1480	13.90	14.30	2.015
1490	14.20	14.60	2.017
1498	14.10	14.50	2.068
Series 2 - Inlet Vacuum = 10" Hg			
1015	10.65	11.00	1.063
1220	11.50	11.87	1.379
1330	13.05	13.44	1.702
1361	12.80	13.19	1.709
1366	12.60	13.00	1.691
1366	12.70	13.10	1.704
1377	13.10	13.50	1.770
1378	13.20	13.59	1.783
1381	13.15	13.54	1.780
1460	13.40	13.80	1.918
1472	14.15	14.55	2.039
1486	14.12	14.52	2.054
1488	14.20	14.61	2.070
1488	14.20	14.61	2.070

[illegible]

[illegible]

[illegible]	[illegible]	[illegible]	[illegible]
[illegible]	[illegible]	[illegible]	[illegible]

[illegible]

[illegible]	[illegible]	[illegible]	[illegible]

Figure XXVI

Photographs of 5" Hg Inlet Vacuum
Scope Presentations

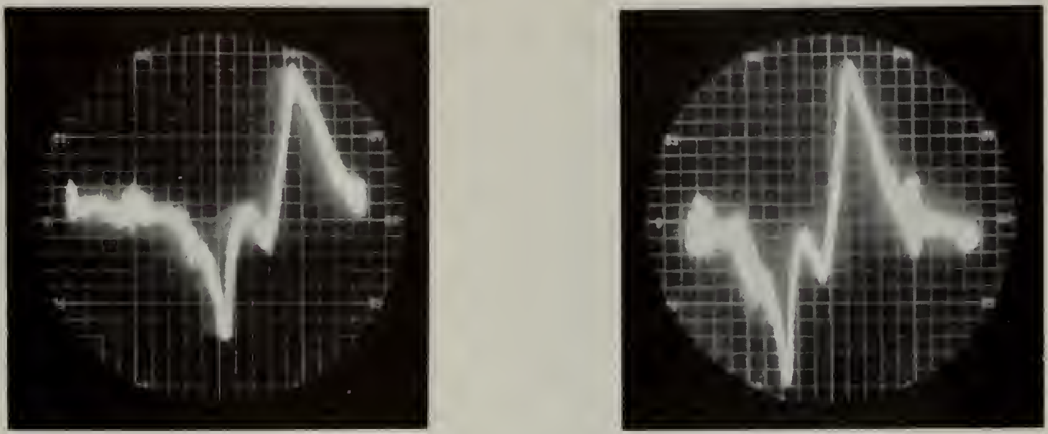

(a)
SPEED = 1170 rpm
Scope Scale: 1 in.= 1 v.

(b)
SPEED = 1270 rpm
Scope Scale: 1 in.= 1 v.

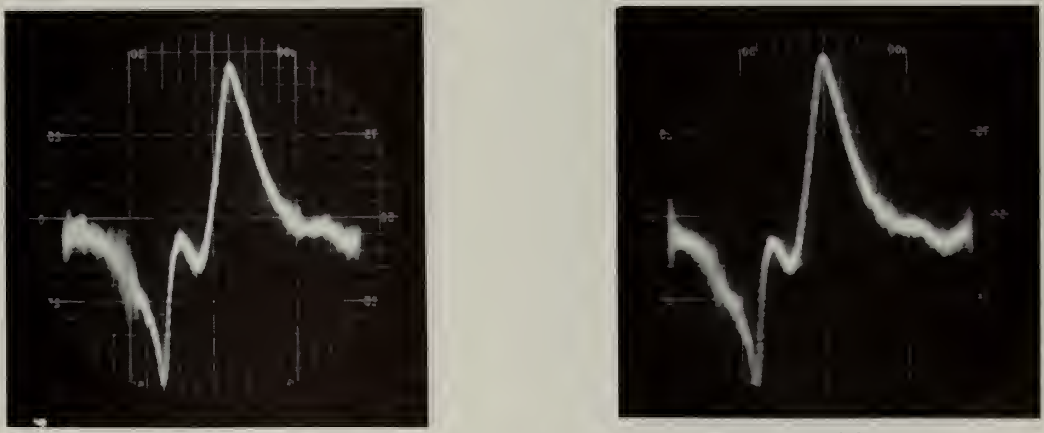

(c)
SPEED = 1360 rpm
Scope Scale: 1 in.= 1 v.

(d)
SPEED = 1420 rpm
Scope Scale: 1 in.= 1 v.

Figure XXVII

Photographs of 10" Hg Inlet Vacuum
Scope Presentations

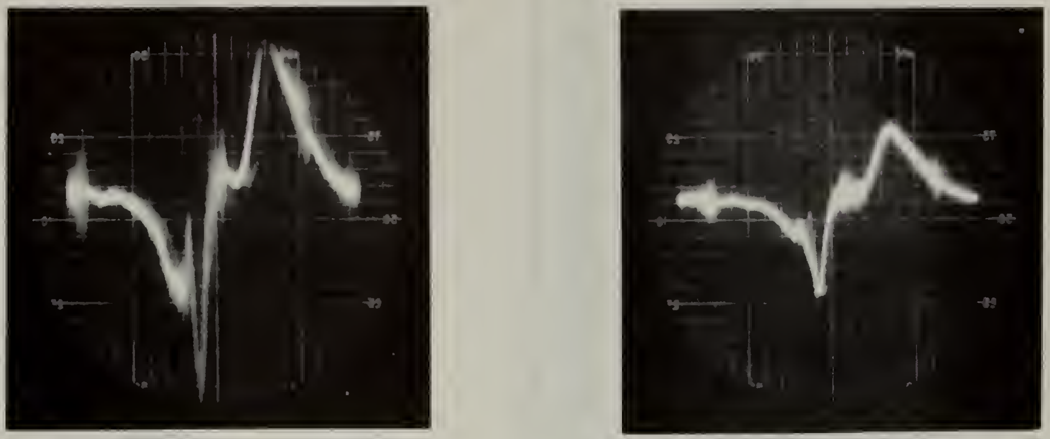

(a)
SPEED = 1015 rpm
Scope Scale: 1 in.= 1 v.

(b)
SPEED = 1220 rpm
Scope Scale: 1 in.= 2.5 v.

(c)
SPEED = 1330 rpm
Scope Scale: 1 in.= 2.5 v.

(d)
SPEED = 1486 rpm
Scope Scale: 1 in.= 2.5 v.

[illegible]

[illegible]

[illegible]

[illegible]

[illegible]

TABLE IV

Data from Experiment 4

Speed (rpm)	Scale Force (lbs)	Actual Force (lbs)	Power (hp)
1000	2.32	2.52	0.240
1000	2.75	2.96	0.282
1040	3.06	3.26	0.330
1050	3.05	3.25	0.325
1052	3.05	3.25	0.326
1060	2.85	3.06	0.306
1060	3.05	3.25	0.328
1062	3.04	3.24	0.328
1062	3.06	3.26	0.330
1062	3.05	3.25	0.329
1100	4.08	4.32	0.452
1110	3.90	4.14	0.437
1110	3.91	4.15	0.439
1115	4.01	4.26	0.452
1120	4.00	4.24	0.452
1120	3.91	4.15	0.442
1124	3.99	4.23	0.453
1130	3.92	4.16	0.447
1132	3.91	4.15	0.447
1170	3.95	4.18	0.466
1174	3.88	4.10	0.458
1175	4.05	4.28	0.479
1180	4.00	4.24	0.476
1180	4.05	4.28	0.481
1180	4.10	4.34	0.487
1180	3.73	3.95	0.444
1184	3.72	3.94	0.444
1184	4.05	4.28	0.482
1190	3.77	4.00	0.453
1194	3.95	4.18	0.475
1200	3.90	4.14	0.473
1205	3.80	4.03	0.462
1210	3.90	4.14	0.477
1210	3.80	4.03	0.464
1235	4.69	4.93	0.580
1244	4.82	5.06	0.599
1245	4.61	4.86	0.576
1250	4.70	4.95	0.589
1250	4.78	5.03	0.599
1260	4.89	5.14	0.617
1260	4.65	4.90	0.588
1265	4.72	4.96	0.597
1265	4.88	5.13	0.618
1266	4.89	5.14	0.619
1266	4.77	5.02	0.605
1270	4.45	4.69	0.567

[illegible]

[illegible]

[illegible]	[illegible]	[illegible]	[illegible]
[illegible]	[illegible]	[illegible]	[illegible]

TABLE IV (contd)

Speed (rpm)	Scale Force (lbs)	Actual Force (lbs)	Power (hp)
1270	4.60	4.84	0.585
1270	4.68	4.92	0.595
1270	4.78	5.03	0.608
1300	3.75	3.99	0.494
1315	4.73	4.97	0.622
1316	4.50	4.74	0.594
1316	4.54	4.78	0.599
1316	4.62	4.85	0.608
1316	4.65	4.89	0.613
1316	4.47	4.61	0.577
1320	4.70	4.94	0.621
1320	4.68	4.92	0.618
1326	4.65	4.89	0.617
1326	4.75	4.99	0.630
1326	4.55	4.79	0.605
1331	4.75	4.99	0.632
1352	5.25	5.49	0.707
1370	5.25	5.49	0.716
1386	5.17	5.42	0.715
1390	5.19	5.44	0.720
1390	5.14	5.39	0.713
1390	5.21	5.46	0.723
1392	5.19	5.44	0.721
1396	5.20	5.45	0.724
1401	5.21	5.46	0.728
1410	5.85	6.11	0.820
1438	5.60	5.86	0.802
1446	5.49	5.74	0.790
1460	5.79	6.05	0.841
1462	5.60	5.86	0.816
1468	6.05	6.31	0.882
1472	5.79	6.05	0.848
1480	5.95	6.20	0.873
1482	6.00	6.26	0.883
1485	5.79	6.05	0.855
1486	5.97	6.23	0.881
1490	6.35	6.61	0.938
1508	6.35	6.61	0.949

[illegible]

[illegible]	[illegible]	[illegible]	[illegible]
[illegible]	[illegible]	[illegible]	[illegible]

Figure XXVIII

Photographs of Scope Presentation
During Experiment 4

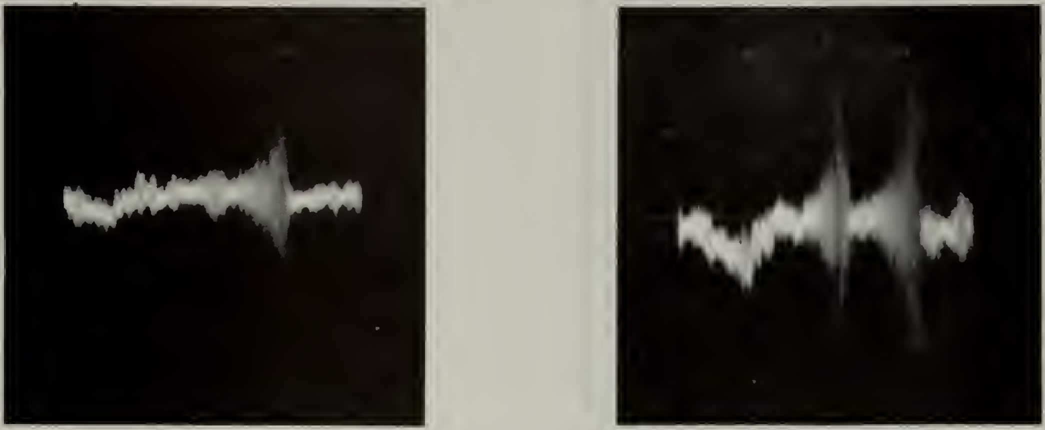

(a)
SPEED = 984 rpm
Scale: 1 in. = 0.25 v.

(b)
SPEED = 1250 rpm
Scale: 1 in. = 0.25 v.

(c)
SPEED = 1366 rpm
Scale: 1 in. = 0.25 v.

[illegible]

[illegible]

[illegible]

[illegible]

TABLE V

Table of Measured Values from Rotor Layout

Rotor Position	Vane End Radius (inches)	Vane Exposure (inches)	Radius to Vane CG (inches)
0	1.945	0.010	1.370
15	1.945	0.020	1.380
30	1.975	0.065	1.405
45	2.020	0.115	1.435
60	2.080	0.185	1.460
75	2.150	0.270	1.515
90	2.235	0.370	1.585
105	2.320	0.470	1.650
120	2.405	0.575	1.730
135	2.485	0.670	1.800
150	2.560	0.750	1.850
165	2.615	0.820	1.900
180	2.650	0.850	1.925
195	2.655	0.855	1.945
210	2.630	0.835	1.922
225	2.580	0.765	1.875
240	2.510	0.690	1.815
255	2.415	0.580	1.730
270	2.310	0.460	1.648
285	2.210	0.345	1.515
300	2.115	0.230	1.490
315	2.035	0.135	1.445
330	1.975	0.065	1.400
345	1.945	0.020	1.390
Average	2.2818	0.4229	1.6325

TABLE VI

Table of Measured Scope Deflections

Rotor Position	Vane	Measured Deflections (inches) Fig. XXVIa	Fig. XXVIb	Fig. XXVIc	Fig. XXVId
Ref	I	-1.55	-1.90	-1.95	-1.95
	II	-0.10	-0.05	-0.05	-0.05
	III	-1.30	-1.25	-1.25	-1.45
	IV	+2.95	+3.20	+3.25	+3.45
Ref + 40	I	-0.70	-0.85	-0.80	-0.85
	II	-0.20	-0.05	-0.15	-0.30
	III	+0.05	-0.10	-0.05	+0.05
	IV	+0.85	+1.00	+1.00	+1.10
Ref + 80	I	-0.10	-0.15	-0.05	-0.15
	II	-0.80	-0.85	-1.05	-1.15
	III	+1.75	+2.30	+2.65	+2.28
	IV	-0.85	-1.30	-1.55	-0.98
Ref + 120	I	-0.10	0	-0.20	-0.30
	II	0	-0.15	+0.05	+0.05
	III	+1.10	+1.10	+1.15	+1.30
	IV	-1.00	-0.95	-1.00	-1.05
Ref + 160	I	-0.60	-0.50	-0.75	-0.80
	II	+0.90	+0.65	+1.35	+1.50
	III	-0.05	+0.15	-0.35	-0.35
	IV	-0.25	-0.30	-0.25	-0.35
Ref + 200	I	-0.20	-0.50	-0.15	-0.35
	II	+1.50	+2.00	+1.65	+2.05
	III	-1.20	-1.40	-1.35	-1.50
	IV	-0.10	-0.10	-0.15	-0.20
Ref + 240	I	+0.30	0	+0.45	+0.40
	II	+0.40	+0.70	+0.45	+0.65
	III	-0.35	-0.40	-0.45	-0.50
	IV	-0.35	-0.30	-0.45	-0.55
Ref + 280	I	+2.10	+3.50	+3.00	+4.10
	II	-1.40	-1.55	-1.55	-1.95
	III	-0.05	-0.10	-0.05	-0.15
	IV	-0.65	-1.85	-1.40	-2.00
Ref + 320	I	+0.70	+0.80	+0.75	+1.00
	II	-0.50	-0.50	-0.55	-0.70
	III	-0.30	-0.20	-0.35	-0.40
	IV	+0.10	-0.10	+0.15	+0.10

TABLE VI (Contd)

Rotor Position	Vane	Measured Deflections (inches)			
		Fig. XXVIIa	Fig. XXVIIb	Fig. XXVIIc	Fig. XXVIId
Ref	I	-1.75	-0.80	-0.90	-0.95
	II	-0.15	-0.05	-0.05	-0.10
	III	-1.25	-0.85	-0.75	-0.75
	IV	+3.15	+1.65	+1.70	+1.80
Ref + 40	I	-1.00	-0.40	-0.40	-0.45
	II	-0.45	-0.20	-0.15	-0.25
	III	+0.65	+0.30	+0.25	+0.30
	IV	+0.80	+0.30	+0.30	+0.40
Ref + 80	I	-0.20	-0.10	-0.10	-0.10
	II	-1.20	-0.60	-0.50	-0.45
	III	+2.70	+1.20	+1.25	+1.25
	IV	-1.30	-0.50	-0.65	-0.70
Ref + 120	I	-0.25	-0.10	-0.15	-0.20
	II	+0.50	+0.15	+0.20	+0.20
	III	+0.95	+0.45	+0.45	+0.55
	IV	-1.20	-0.50	-0.50	-0.55
Ref + 160	I	-1.10	-0.35	-0.30	-0.50
	II	+2.05	+0.80	+0.90	+1.10
	III	-0.65	-0.40	-0.45	-0.45
	IV	-0.30	-0.05	-0.15	-0.15
Ref + 200	I	+0.10	0	+0.10	-0.50
	II	+1.30	+0.70	+0.60	+1.35
	III	-1.15	-0.60	-0.55	-0.70
	IV	-0.25	-0.10	-0.15	-0.15
Ref + 240	I	+1.20	+0.55	+0.75	+0.60
	II	+0.15	0	-0.15	+0.10
	III	-0.50	-0.15	-0.20	-0.30
	IV	-0.85	-0.40	-0.40	-0.40
Ref + 280	I	+3.60	+1.55	+1.55	+2.00
	II	-1.55	-0.75	-0.65	-0.90
	III	-0.10	-0.05	-0.10	-0.10
	IV	-1.95	-0.75	-0.75	-1.00
Ref + 320	I	+0.65	+0.15	+0.15	+0.20
	II	-0.75	-0.25	-0.25	-0.35
	III	-0.70	-0.25	-0.35	-0.30
	IV	+0.80	+0.35	+0.45	+0.45

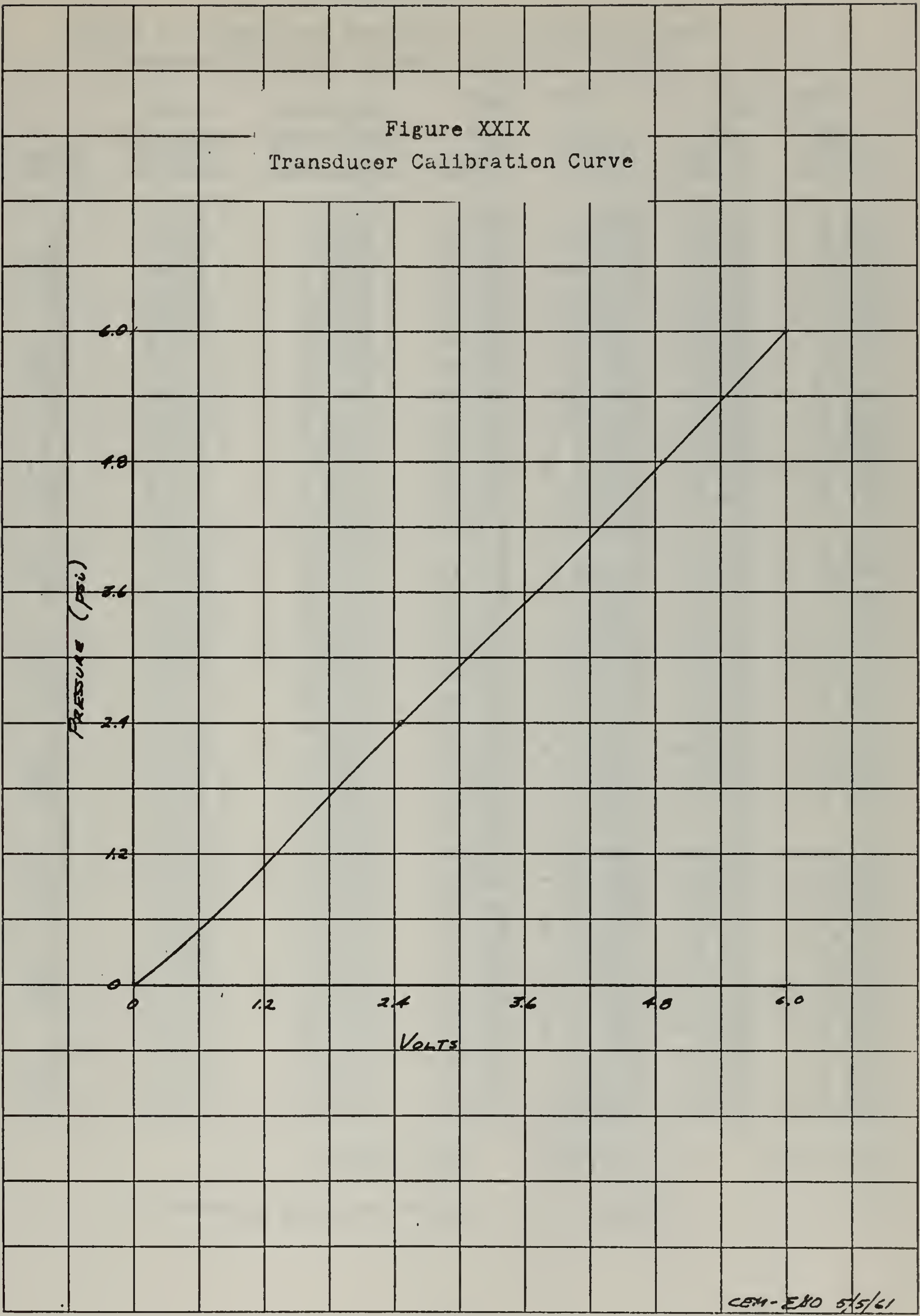

Figure XXIX
Transducer Calibration Curve

CEM-EMO 5/5/61

TABLE VII

Table of Computed Pressure Differences and Pressure Forces, Inlet Vacuum = 5" Hg.

Rotor Position	Vane	Vane Exposure (inch)	Exposed Vane Area (sq. in.)	Fig. XXVIa Δp (psi)	 $A\Delta p$ (lbs)	Fig. XXVIb Δp (psi)	 $A\Delta p$ (lbs)
Ref	I	0.28	1.741	-1.63	- 2.838	-1.96	- 3.412
	II	0.04	0.249	-0.14	- 0.035	-0.06	- 0.015
	III	0.53	3.296	-1.40	- 4.614	-1.36	- 4.483
	IV	0.86	5.348	+3.04	+16.258	+3.29	+17.595
Ref+40	I	0.06	0.373	-0.83	- 0.310	-0.98	- 0.366
	II	0.21	1.306	-0.26	- 0.340	-0.06	- 0.078
	III	0.77	4.788	+0.06	+ 0.287	-0.14	- 0.670
	IV	0.67	4.167	+0.98	+ 4.084	+1.12	+ 4.667
Ref+80	I	0.025	0.155	-0.14	- 0.022	-0.20	- 0.031
	II	0.46	2.861	-0.94	- 2.689	-0.98	- 2.804
	III	0.87	5.410	+1.81	+ 9.792	+2.35	+12.714
	IV	0.37	2.310	-0.98	- 2.264	-1.40	- 3.234
Ref+120	I	0.16	0.995	-0.14	- 0.139	0	0
	II	0.72	4.478	0	0	-0.20	- 0.896
	III	0.78	4.851	+1.22	+ 5.918	+1.22	+ 5.918
	IV	0.10	0.622	-1.12	- 0.697	-1.07	- 0.666
Ref+160	I	0.415	2.581	-0.72	- 1.858	-0.61	- 1.574
	II	0.85	5.286	+1.04	+ 5.497	+0.78	+ 4.123
	III	0.45	2.798	-0.06	- 0.168	+0.20	+ 0.560
	IV	0.01	0.062	-0.34	- 0.021	-0.39	- 0.024
Ref+200	I	0.66	4.104	-0.26	- 1.067	-0.61	- 2.503
	II	0.78	4.851	+1.59	+ 7.713	+2.05	+ 9.945
	III	0.15	0.933	-1.31	- 1.222	-1.50	- 1.400
	IV	0.11	0.684	-0.14	- 0.096	-0.14	- 0.096
Ref+240	I	0.84	5.224	+0.39	+ 2.037	0	0
	II	0.53	3.296	+0.50	+ 1.648	+0.83	+ 2.736
	III	0.015	0.093	-0.46	- 0.043	-0.50	- 0.047
	IV	0.33	2.052	-0.46	- 0.944	-0.39	- 0.800
Ref+280	I	0.83	5.162	+2.15	+11.098	+3.60	+18.583
	II	0.215	1.337	-1.50	- 2.006	-1.63	- 2.179
	III	0.06	0.373	-0.06	- 0.022	-0.14	- 0.052
	IV	0.59	3.669	-0.78	- 2.862	-1.90	- 6.971
Ref+320	I	0.61	3.793	+0.83	+ 3.148	+0.94	+ 3.565
	II	0.03	0.187	-0.61	- 0.114	-0.61	- 0.114
	III	0.265	1.648	-0.39	- 0.643	-0.26	- 0.429
	IV	0.81	5.037	-0.14	+ 0.705	-0.14	- 0.705
				Total $A\Delta p$	+43.171		+46.857
			Average $A\Delta p$ per vane		+ 1.1992		+ 1.3017

TABLE VII (contd)

Rotor Position	Vane	Vane Exposure (inch)	Exposed Vane Area (sq. in.)	Fig. XXVIc Δp (psi)	$A\Delta p$ (lbs)	Fig. XXVId Δp (psi)	$A\Delta p$ (lbs)
Ref	I	0.28	1.741	-2.00	- 3.482	-2.00	- 3.482
	II	0.04	0.249	-0.06	- 0.015	-0.06	- 0.015
	III	0.53	3.296	-1.36	- 4.483	-1.55	- 5.109
	IV	0.86	5.348	+3.34	+17.862	+3.54	+18.932
Ref+40	I	0.06	0.373	-0.94	- 0.351	-0.98	- 0.366
	II	0.21	1.306	-0.20	- 0.261	-0.39	- 0.509
	III	0.77	4.788	-0.06	+ 0.287	+0.06	+ 0.287
	IV	0.67	4.167	+1.12	+ 4.667	+1.22	+ 5.084
Ref+80	I	0.025	0.155	-0.06	- 0.009	-0.20	- 0.031
	II	0.46	2.861	-1.16	- 3.319	-1.26	- 3.605
	III	0.87	5.410	+2.72	+14.715	+2.34	+12.659
	IV	0.37	2.310	-1.63	- 3.765	-1.10	- 2.541
Ref+120	I	0.16	0.995	-0.26	- 0.259	-0.39	- 0.388
	II	0.72	4.478	+0.06	+ 0.269	+0.06	+ 0.269
	III	0.78	4.851	+1.26	+ 6.112	+1.40	+ 6.791
	IV	0.10	0.622	-1.12	- 0.697	-1.16	- 0.722
Ref+160	I	0.415	2.581	-0.88	- 2.271	-0.94	- 2.426
	II	0.85	5.286	+1.44	+ 7.612	+1.59	+ 8.405
	III	0.45	2.798	-0.46	- 1.287	-0.46	- 1.287
	IV	0.01	0.062	-0.34	- 0.021	-0.46	- 0.029
Ref+200	I	0.66	4.104	-0.20	- 0.821	-0.46	- 1.888
	II	0.78	4.851	+1.72	+ 8.344	+2.10	+10.187
	III	0.15	0.933	-1.44	- 1.344	-1.59	- 1.483
	IV	0.11	0.684	-0.20	- 0.137	-0.26	- 0.178
Ref+240	I	0.84	5.224	+0.56	+ 2.925	+0.50	+ 2.612
	II	0.53	3.296	+0.56	+ 1.846	+0.78	+ 2.571
	III	0.015	0.093	-0.56	- 0.052	-0.61	- 0.057
	IV	0.33	2.052	-0.56	- 1.149	-0.66	- 1.354
Ref+280	I	0.83	5.162	+3.09	+15.951	+4.19	+21.629
	II	0.215	1.337	-1.63	- 2.179	-2.00	- 2.674
	III	0.06	0.373	-0.06	- 0.022	-0.20	- 0.075
	IV	0.59	3.669	-1.50	- 5.504	-2.06	- 7.558
Ref+320	I	0.61	3.793	+0.88	+ 3.339	+1.12	+ 4.248
	II	0.03	0.187	-0.66	- 0.123	-0.83	- 0.155
	III	0.265	1.648	-0.46	- 0.758	-0.50	- 0.824
	IV	0.81	5.037	+0.20	+ 1.008	+0.14	+ 0.705
			Total $A\Delta p$		+52.628		+57.623
		Average $A\Delta p$ per vane			+ 1.4619		+ 1.6006

TABLE VIII

Table of Computed Pressure Differences and
Pressure Forces, Inlet Vacuum = 10" Hg.

				Fig.XXVIIa		Fig.XXVIIb	
Rotor Position	Vane	Vane Exposure (inch)	Exposed Vane Area (sq. in.)	Δp (psi)	$A\Delta p$ (lbs)	Δp (psi)	$A\Delta p$ (lbs)
Ref	I	0.28	1.741	-1.82	- 3.169	-2.06	- 3.586
	II	0.04	0.249	-0.20	- 0.050	-0.16	- 0.040
	III	0.53	3.296	-1.36	- 4.483	-2.06	- 6.790
	IV	0.86	5.348	+3.25	+17.381	+4.20	+22.462
Ref+40	I	0.06	0.373	-1.12	- 0.418	-1.12	- 0.418
	II	0.21	1.306	-0.56	- 0.731	-0.62	- 0.810
	III	0.77	4.788	+0.77	+ 3.687	+0.88	+ 4.213
	IV	0.67	4.167	+0.94	+ 3.917	+0.88	+ 3.667
Ref+80	I	0.025	0.155	-0.26	- 0.040	-0.32	- 0.050
	II	0.46	2.861	-1.31	- 3.748	-1.59	- 4.549
	III	0.87	5.410	+2.78	+15.040	+3.09	+16.717
	IV	0.37	2.310	-1.40	- 3.221	-1.36	- 3.129
Ref+120	I	0.16	0.995	-0.32	- 0.318	-0.32	- 0.318
	II	0.72	4.478	+0.62	+ 2.776	+0.48	+ 2.149
	III	0.78	4.851	+1.07	+ 5.191	+1.24	+ 6.015
	IV	0.10	0.622	-1.31	- 0.815	-1.36	- 0.846
Ref+160	I	0.415	2.581	-1.22	- 3.149	-1.00	- 2.581
	II	0.85	5.286	+2.10	+11.101	+2.06	+10.889
	III	0.45	2.798	-0.77	- 2.154	-1.12	- 3.134
	IV	0.01	0.062	-0.38	- 0.024	-0.16	- 0.010
Ref+200	I	0.66	4.104	+0.14	+ 0.575	0	0
	II	0.78	4.851	+1.40	+ 6.791	+1.82	+ 8.829
	III	0.15	0.933	-1.26	- 1.176	-1.59	- 1.483
	IV	0.11	0.684	-0.32	- 0.219	-0.32	- 0.219
Ref+240	I	0.84	5.224	+1.31	+ 6.843	+1.48	+ 7.732
	II	0.53	3.296	+0.20	+ 0.659	0	0
	III	0.015	0.093	-0.62	- 0.058	-0.48	- 0.045
	IV	0.33	2.052	-0.98	- 2.011	-1.12	- 2.298
Ref+280	I	0.83	5.162	+3.70	+19.099	+3.96	+20.442
	II	0.215	1.337	-1.63	- 2.179	-1.94	- 2.594
	III	0.06	0.373	-0.14	- 0.052	-0.16	- 0.060
	IV	0.59	3.669	-2.00	- 7.338	-1.94	- 7.118
Ref+320	I	0.61	3.793	+0.77	+ 2.921	+0.48	+ 1.821
	II	0.03	0.187	-0.88	- 0.165	-0.74	- 0.138
	III	0.265	1.648	-0.84	- 1.384	-0.74	- 1.220
	IV	0.81	5.037	+0.94	+ 4.735	+1.00	+ 5.037
			Total $A\Delta p$		+62.654		+68.537
			Average $A\Delta p$ per vane		+1.7404		+1.9038

[illegible]

[illegible]
[illegible]

[illegible]

[illegible]
[illegible]

TABLE VIII (contd)

Rotor Position	Vane	Vane Exposure (inch)	Exposed Vane Area (sq. in.)	Fig.XXVIIc		Fig.XXVIId	
				Δp (psi)	$A\Delta p$ (lbs)	Δp (psi)	$A\Delta p$ (lbs)
Ref	I	0.28	1.741	-2.30	- 4.004	-2.43	- 4.236
	II	0.04	0.249	-0.16	- 0.040	-0.32	- 0.080
	III	0.53	3.296	-1.94	- 6.394	-1.94	- 6.394
	IV	0.86	5.348	+4.34	+23.210	+4.57	+24.440
Ref+40	I	0.06	0.373	-1.12	- 0.418	-1.24	- 0.463
	II	0.21	1.306	-0.48	- 0.627	-0.74	- 0.966
	III	0.77	4.788	+0.74	+ 3.543	+0.88	+ 4.213
	IV	0.67	4.167	+0.88	+ 3.667	+1.12	+ 4.667
Ref+80	I	0.025	0.155	-0.32	- 0.050	-0.32	- 0.050
	II	0.46	2.861	-1.36	- 3.891	-1.24	- 3.548
	III	0.87	5.410	+3.20	+17.312	+3.20	+17.312
	IV	0.37	2.310	-1.70	- 3.912	-1.82	- 4.188
Ref+120	I	0.16	0.995	-0.48	- 0.478	-0.62	- 0.617
	II	0.72	4.478	+0.62	+ 2.776	+0.62	+ 2.776
	III	0.78	4.851	+1.24	+ 6.015	+1.48	+ 7.179
	IV	0.10	0.622	-1.36	- 0.846	-1.48	- 0.921
Ref+160	I	0.415	2.581	-0.88	- 2.271	-1.36	- 3.510
	II	0.85	5.286	+2.30	+12.158	+2.83	+14.959
	III	0.45	2.798	-1.24	- 3.470	-1.24	- 3.470
	IV	0.01	0.062	-0.48	- 0.030	-0.48	- 0.030
Ref+200	I	0.66	4.104	+0.32	+ 1.313	-1.36	- 5.581
	II	0.78	4.851	+1.59	+ 7.713	+3.48	+16.881
	III	0.15	0.933	-1.48	- 1.381	-1.82	- 1.698
	IV	0.11	0.684	-0.48	- 0.328	-0.48	- 0.328
Ref+240	I	0.84	5.224	+1.94	+10.135	+1.59	+ 8.306
	II	0.53	3.296	-0.48	- 1.582	+0.32	+ 1.055
	III	0.015	0.093	-0.62	- 0.058	-0.88	- 0.082
	IV	0.33	2.052	-1.12	- 2.298	-1.12	- 2.298
Ref+280	I	0.83	5.162	+3.96	+20.442	+5.05	+26.068
	II	0.215	1.337	-1.70	- 2.273	-2.30	- 3.075
	III	0.06	0.373	-0.32	- 0.119	-0.32	- 0.119
	IV	0.59	3.669	-1.94	- 7.118	-2.56	- 9.393
Ref+320	I	0.61	3.793	+0.48	+ 1.821	+0.62	+ 2.352
	II	0.03	0.187	-0.74	- 0.138	-1.00	- 0.187
	III	0.265	1.648	-1.00	- 1.648	-0.88	- 1.450
	IV	0.81	5.037	+1.24	+ 6.246	+1.24	+ 6.246
			Total $A\Delta p$		+72.976		+83.768
		Average $A\Delta p$ per vane			+2.0271		+2.3269

TABLE IX

Table of Calculated Values for f_{sf}, f_{rf}, P_{sfd}, and P_{rfd}

Speed (rpm)	f_{sf}	f_{rf}	P_{sfd} (hp)	P_{rfd} (hp)
1015	0.1317	0.4068	0.2039	0.0711
1170	0.1183	0.4561	0.3079	0.1331
1220	0.1157	0.4576	0.3393	0.1497
1270	0.1134	0.4695	0.3705	0.1930
1330	0.1093	0.4838	0.4387	0.2163
1360	0.1075	0.4818	0.4557	0.2263
1420	0.1034	0.4932	0.5058	0.2662
1486	0.1048	0.4867	0.5810	0.2980

[illegible]

[illegible]

[illegible]

[illegible]	[illegible]	[illegible]	[illegible]	[illegible]
[illegible]	[illegible]	[illegible]	[illegible]	[illegible]
[illegible]	[illegible]	[illegible]	[illegible]	[illegible]
[illegible]	[illegible]	[illegible]	[illegible]	[illegible]
[illegible]	[illegible]	[illegible]	[illegible]	[illegible]
[illegible]	[illegible]	[illegible]	[illegible]	[illegible]
[illegible]	[illegible]	[illegible]	[illegible]	[illegible]
[illegible]	[illegible]	[illegible]	[illegible]	[illegible]
[illegible]	[illegible]	[illegible]	[illegible]	[illegible]

TABLE X

Table of Calculated Values for P_{sf} and P_{rf}

Series 1 Inlet Vacuum = 5" Hg.

Speed (rpm)	P_{sf} (hp)	P_{rf} (hp)
1170	0.3557	0.1718
1270	0.4427	0.2266
1360	0.5239	0.2875
1420	0.5841	0.3396

Series 2 Inlet Vacuum = 10" Hg.

Speed (rpm)	P_{sf} (hp)	P_{rf} (hp)
1015	0.2573	0.1096
1220	0.4167	0.2140
1330	0.5343	0.3008
1486	0.6985	0.4065

APPENDIX C

Sample Calculations

The procedure for calculating f_{sf}, f_{rf}, P_{sfd}, P_{rfd}, P_{sf}, and P_{rf} will be illustrated by calculating these values for the conditions of:

Speed = N = 1170 rpm.

Inlet Vacuum = 5" Hg.

Eqn. (2) $N_c = \frac{N}{1.0082} = \frac{1170}{1.0082}$

$N_c = 1161$ rpm.

Eqn. (4) $(P_{sfd})_{nc} = (P_2)_{nc} - (P_1)_n$

$= 0.160 - 0.0155$

$(P_{sfd})_{nc} = 0.1445$ hp.

Eqn. (7) $G_c = \frac{w}{g}\left(\frac{2\pi N_c}{60}\right)^2\left(\frac{R_{gc}}{12}\right)\cos\beta_c$

$= \left(\frac{0.131}{32.2}\right)\left(\frac{2\pi}{60}\right)^2(1161)^2\left(\frac{1.645}{12}\right)(0.6947)$

$G_c = 8.2577\ (0.6947)$

$\frac{G_c}{\cos\lambda_c} = \frac{8.2577\ (0.6947)}{0.8572}$

$\frac{G_c}{\cos\lambda_c} = 6.6920$ lbs.

Eqn. (3) $V_c = \left(\frac{2\pi N_c}{60}\right)\left(\frac{R_{vc}}{12}\right)$

$V_c = 23.313$ ft/sec.

Eqn. (9) $I_{cd} = \frac{G_c}{\cos\lambda_c} + \frac{137.5(P_{sfd})_{nc}\tan\lambda_c}{V_c}$

$= 6.6920 + \frac{19.8688(0.6009)}{23.313}$

$I_{cd} = 7.204$ lbs.

Eqn. (8) rewritten $f_{sf} = \frac{137.5(P_{sfd})_{nc}}{I_{cd}V_c}$

$= \frac{19.8688}{(7.204)(23.313)}$

$\underline{\underline{f_{sf} = 0.1183}}$

Eqn. (11) $$F_a = \frac{w}{g}\left(\frac{2\pi N}{60}\right)^2\left(\frac{R_g}{12}\right)\cos\beta$$

$$= \left(\frac{0.131}{32.2}\right)\left(\frac{2\pi}{60}\right)^2(1170)^2\left(\frac{1.6325}{12}\right)(0.6756)$$

$$= 8.3345(0.6756)$$

$$F_a = 5.631 \text{ lbs.}$$

Eqn. (16) $$V_r = \frac{N\,e\sec\lambda}{180}$$

$$= \frac{1170(0.3715)(1.179)}{180}$$

$$= 1170(0.002433)$$

$$V_r = 2.847 \text{ ft/sec.}$$

$$(P_4)_n - (P_1)_n = 0.456 - 0.0155$$

$$(P_4)_n - (P_1)n = 0.4405 \text{ hp.}$$

Eqn. (18) $$f_{rf}(R_1+R_2) = \frac{137.5(P_4-P_1)(\cos\lambda - f_{sf}\sin\lambda) - f_{sf}VF_a}{f_{sf}\ V + V_r(\cos\lambda - f_{sf}\ \sin\lambda)}$$

$$= \frac{137.5(0.4405)(0.848-0.1183 \times 0.5299)-0.1183(23.313)(5.631)}{0.1183(23.313)+2.847(0.848-0.1183 \times 0.5299)}$$

$$= 6.427 \text{ lbs.}$$

Eqn. (12) $$F_{rd} = \frac{F_a + f_{rf}(R_1 + R_2)}{\cos\lambda - f_{sf}\ \sin\lambda}$$

$$= \frac{5.631 + 6.427}{0.848 - 0.1183(0.5299)}$$

$$F_{rd} = 15.353 \text{ lbs.}$$

Eqn. (20) $$H_{rd} = F_{rd}\ (\sin\lambda + f_{sf}\ \cos\lambda)$$

$$= 15.353\ [0.5299 + (0.1183)(0.848)]$$

$$= 9.675 \text{ lbs.}$$

Eqn. (21) $$H_c = \frac{w}{g}\left(\frac{2\pi N}{60}\right)^2\left(\frac{R_g}{12}\right)\sin\beta$$

$$= 8.3345(0.7373)$$

$$H_c = 6.145 \text{ lbs.}$$

Eqn. (19) $R_1+R_2 = 1.6688\ H_{rd} - 0.3344\ H_c$

$= 1.6688\ (9.675)-0.3344(6.145)$

$R_1+R_2 = 14.092$ lbs.

Eqn. (22) $f_{rf} = \dfrac{f_{rf}(R_1+R_2)}{R_1 + R_2}$

$= \dfrac{6.4273}{14.0915}$

$\underline{\underline{f_{rf} = 0.4561}}$

Eqn. (13) $P_{sfd} = \dfrac{4 f_{sf}\ F_{rd}\ V}{550}$

$= \dfrac{4(0.1183)(15.353)(23.313)}{550}$

$\underline{\underline{P_{sfd} = 0.3079\ \text{hp.}}}$

Eqn. (15) $P_{rfd} = \dfrac{4\ f_{rf}(R_1 + R_2)V_r}{550}$

$= \dfrac{4(0.4561)(14.092)(2.847)}{550}$

$\underline{\underline{P_{rfd} = 0.1331\ \text{hp.}}}$

$H_p = 1.1992$ lbs. from Table VII

Eqn. (25) $F_r = \dfrac{F_a+1.3344\ f_{rf}\ H_p - 0.3344\ f_{rf}\ H_c}{(\cos\lambda-f_{sf}\ \sin\lambda)-1.6688(\sin\lambda+f_{sf}\ \cos\lambda)f_{rf}}$

$= \dfrac{5.631+1.3344(.4561)(1.1992)-0.3344(.4561)(6.145)}{0.848-0.1183(0.5299)-1.6688[0.5299+0.1183(0.848)](.4561)}$

$F_r = 17.735$ lbs.

Eqn. (24) $R_3+R_4 = 1.6688(\sin\lambda+f_{sf}\cos\lambda)F_r+1.3344H_p-0.3344H_c$

$=1.6688[0.5299+0.1183(0.848)](17.735)+1.3344(1.1992)-0.3344(6.145)$

$R_3+R_4 = 18.187$ lbs.

Eqn. (26) $P_{sf} = \dfrac{4\ f_{sf}\ F_r\ V}{550}$

$= \dfrac{4(0.1183)(17.735)(23.313)}{550}$

$\underline{\underline{P_{sf} = 0.3557\ \text{hp.}}}$

Eqn. (27) $$P_{rf} = \frac{4\ f_{rf}(R_3+R_4)V_r}{550}$$

$$= \frac{4(0.4561)(18.187)(2.847)}{550}$$

$$\underline{\underline{P_{rf} = 0.1718 \text{ hp.}}}$$

APPENDIX D

Literature Citations

1. ARCHARD, J. F., "The Temperature of Rubbing Surfaces," Wear, Vol. 2, October, 1959.

2. BAILEY, G. W. and WRIGHT, E. A., "Frictional Resistance with Pressure Gradient," M.S. Thesis, N. A. Dept., 1939.

3. BOWDEN, F. P. and TABOR, D., The Friction and Lubrication of Solids, Oxford at the Clarendon Press, 1954.

4. BRANSFORD, E. O. and STEIN, R. A., "Design Control of Overcompression in Rotary-Vane Compressors," Journal of Engineering for Power, Vol. 82, July, 1960.

5. DEL VALLE PENA, A., "Frictional Behavior of Metal Interfaces," M.S. Thesis, M. E. Dept., 1957.

6. FROEDE, W. G., "The NSU-Wankel Rotating Combustion Engine," for presentation at the 1961 SAE International Congress and Exposition of Automotive Engineering, Society of Automotive Engineering, Preprint, 1961.

7. GEMANT, A., Frictional Phenomena, Brooklyn Chemical Pub. Co., 1950.

8. HEYMANN, F. J., "An Investigation of Solid Friction at Very Low Sliding Speeds," M.S. Thesis, M. E. Dept., 1953.

9. KINGSBURY, E. P., "The Influence of Bulk Temperature on Metallic Friction and Wear," Sc.D. Thesis, M. E. Dept., 1957.

10. KRISTAL, F. A. and ANNETT, F. A., Pumps, McGraw-Hill Book Co., Inc., 1940.

11. McLEOD, M. K., "Engine Friction," The Automobile Engineer, Vol. 27, February, 1937.

12. MORDIKE, B. L., "The Mechanical Properties and Friction of Carbon and Graphite at High Temperatures," Proceedings of the Fourth Conference on Carbon, Pergamon Press, 1960.

13. SHAW, M. C. and MACKS, E. F., Analysis and Lubrication of Bearings, McGraw-Hill Book Co., Inc., 1949.

14. STEKLY, Z. J. J., "Losses in the Rotor of an Induction Motor as Determined by its Rate of Temperature Rise," M.S. Thesis, M. E. Dept., 1955.

15. TEDHOLM, C. E. and WILLIAMS, R. E., "The Statistical Nature of Friction," Nav. E. Thesis, N.A. Dept., 1953.